

The importance of vehicle emissions as a source of atmospheric ammonia in the megacity of Shanghai

Y. H. Chang^{1, 2}, Z. Zou³, C. R. Deng^{1, 2}, K. Huang^{1, 2, 5}, J. L. Collett Jr.⁴, J. Lin¹, and G. Zhuang^{1, 2}

¹Center for Atmospheric Chemistry Study, Department of Environmental Science and Engineering, Fudan University, Shanghai 200433, China

²Shanghai Key Laboratory of Atmospheric Particle Pollution and Prevention (LAP³), Department of Environmental Science and Engineering, Fudan University, Shanghai 200433, China

³Pudong New Area Environmental Monitoring Station, Shanghai 200135, China

⁴Department of Atmospheric Science, Colorado State University, Fort Collins, CO 80523, USA

⁵Department of Civil and Environmental Engineering, The University of Tennessee, Knoxville, TN 37996, USA

Correspondence to: C. R. Deng (congruideng@fudan.edu.cn) and G. Zhuang (gzhuang@fudan.edu.cn)

Abstract

Agricultural activities are a major source contributing to NH_3 concentrations in Shanghai and most other regions of China; however, there is a long-standing and ongoing controversy regarding the contributions of vehicle-emitted NH_3 to the urban atmosphere. From April 2014 to April 2015, we conducted measurements of a wide range of gases (including NH_3) and the chemical properties of $\text{PM}_{2.5}$ at hourly resolution at a Shanghai urban supersite. This large dataset shows NH_3 pollution events, lasting several hours with concentrations four times the annual average of $5.3 \mu\text{g m}^{-3}$, caused by the burning of crop residues in spring. There are also generally higher NH_3 concentrations (mean $\pm 1\sigma$) in summer ($7.3 \pm 4.9 \mu\text{g m}^{-3}$; $n=2181$) because of intensive emissions from temperature-dependent agricultural sources. However, the NH_3 concentration in summer was only an average of $2.4 \mu\text{g m}^{-3}$ or 41% higher than the average NH_3 concentration of other seasons. Furthermore, the NH_3 concentration in winter ($5.0 \pm 3.7 \mu\text{g m}^{-3}$; $n=2113$) was similar to that in spring ($5.1 \pm 3.8 \mu\text{g m}^{-3}$; $n=2198$) but slightly higher, on average, than that in autumn ($4.5 \pm 2.3 \mu\text{g m}^{-3}$; $n=1949$). Moreover, other meteorological parameters like planetary boundary layer height and relative humidity were not major factors affecting seasonal NH_3 concentrations. These findings suggest that there may be some climate-independent NH_3 sources present in the Shanghai urban area. Independent of season, the concentrations of both NH_3 and CO present a marked bimodal diurnal profile, with maxima in the morning and the evening. A spatial analysis suggests that elevated concentrations of NH_3 are often associated with transport from regions west-northwest and east-southeast of the city, areas with dense road systems. The spatial origin of NH_3 and the diurnal concentration profile together suggest the importance of vehicle-derived NH_3 associated with daily commuting in the urban environment. To further examine vehicular NH_3 emissions and transport, sampling of the NH_3 concentration was performed in (from the entrance to the exit of the tunnel) and out (along a roadside transect spanning 310 m perpendicular to the tunnel) of a heavily trafficked urban tunnel during the spring 2014. NH_3 concentrations in the tunnel exit were over 5 and 11 times higher than those in the tunnel entrance and in the ambient air, respectively. Based on the derived mileage-based NH_3 emission factor of 28 mg km^{-1} , a population of 3.04 million vehicles in Shanghai produced around 1300 t NH_3 in 2014, which accounts for 12% of total NH_3 emissions in the urban area. Collectively, our results clearly show that vehicle emissions associated with combustion are an important NH_3 source in Shanghai urban areas and may have potential implications for $\text{PM}_{2.5}$ pollution in the urban atmosphere.

1 Introduction

Ammonia (NH_3) is one of the most abundant nitrogen-containing substances and the principal reduced nitrogen component in the atmosphere. It plays a strong role in local and regional scale tropospheric chemistry and air quality by serving as a precursor to particulate ammonium (pNH_4^+) (Seinfeld and Pandis, 2012). Although major efforts have been made towards regulating NO_x and SO_2 emissions to improve air quality in China (Wang et al., 2014; Zhao et al., 2013), a major portion of the nation's population presently lives in environments of non-compliance with national standards for fine particulate matter ($\text{PM}_{2.5}$, representing particles with aerodynamic diameters smaller than 2.5 microns) (Huang et al., 2014; Lin et al., 2010; Ma et al., 2014; Ma et al., 2015). NH_3 emission reduction has been proposed as a cost-effective strategy to lower ambient $\text{PM}_{2.5}$ levels (Heald et al., 2012; Pinder et al., 2007; Wang et al., 2011; Wang et al., 2013; Ye et al., 2011). However, the emission sources of NH_3 and their relative contributions to ambient concentrations, especially in urban atmospheres, remain uncertain (Chang, 2014; Felix et al., 2014; Yao et al., 2013).

Emission sources of NH_3 have been previously reviewed (e.g., Asman et al., 1998; Reis et al., 2009; Sutton et al., 2008). Major sources include volatilization of N-containing fertilizers and excreta from animal husbandry, which together contribute over 80% of total global NH_3 emissions (Bouwman et al., 1997; Clarisse et al., 2009; Olivier et al., 1998; Schlesinger and Hartley, 1992). Thus it is not surprising that previous investigations of NH_3 emissions were mainly performed adjacent to dairy operations (Mount et al., 2002), animal housing (Gay et al., 2003), livestock facilities (Kawashima and Yonemura, 2001), slurry lagoons (Aneja et al., 2000), pit latrines (Rodhe et al., 2004), and croplands (Yan et al., 2003), where elevated levels of NH_3 are often observed. Varying significantly in time and space, biomass burning (including agricultural waste, savanna and forest fires) may contribute up to 12% of the global NH_3 emissions flux (Behera et al., 2013; Lamarque et al., 2010). Despite the focus on ammonia sources mainly from agricultural and rural environments, a number of studies reveal that ambient NH_3 concentrations in urban areas can be comparable to (Cao et al., 2009; Stanier et al., 2012) or even higher than (Bettez et al., 2013; Meng et al., 2011; Singh and Kulshrestha, 2014) those in rural areas. These observations strongly suggest that there must be other non-agricultural NH_3 sources present in urban areas.

Starting in the 1980s, the introduction of three-way catalytic converters (TWCs) on automobiles dramatically mitigated pollutant emissions from vehicle tailpipes (Shelef and

McCabe, 2000). An unwanted side effect of the use of TWCs for gasoline powered vehicles and selective catalytic reduction (SCR) for control of nitrogen oxides emissions from diesel powered vehicles, has been an increase in NH_3 emissions from motor vehicles, a significant source of non-agricultural NH_3 that has been documented directly through laboratory dynamometer studies (Durbin et al., 2002; Heeb et al., 2008; Heeb et al., 2006; Huai et al., 2005; Livingston et al., 2009; Suarez-Bertoa et al., 2014; Suarez-Bertoa et al., 2015) and on-road measurements (including mobile chase systems and tunnel tests) (Brito et al., 2013; Fraser and Cass, 1998; Kean et al., 2009; Liu et al., 2014; Moeckli et al., 1996; Pierson and Brachaczek, 1983; Pierson et al., 1996; Sun et al., 2014), or indirectly through correlation analysis between ambient NH_3 concentrations and other recognized traffic tracers (e.g., CO , NO_x) (Bishop and Stedman, 2015; Gong et al., 2011; Gong et al., 2013; Ianniello et al., 2010; Nowak et al., 2010; Pandolfi et al., 2012; Phan et al., 2013; Reche et al., 2012). In the U.S., it is estimated that 5% of the national NH_3 emissions are due to motor vehicles (Kean et al., 2009), while this figure is estimated at 12% for the UK (Sutton et al., 2000), with almost all the remaining NH_3 coming from agricultural processes. At a regional level, motor vehicle emissions make a small contribution to the total. Nevertheless, they are locally concentrated in urban areas where agricultural sources of NH_3 are mostly absent. Therefore, a disproportionately greater impact of motor vehicles on the urban NH_3 budget and subsequent secondary $\text{PM}_{2.5}$ formation can be expected (Chang, 2014). On the other hand, we notice that several important studies did not detect evidence of an influence of on-road traffic on ambient NH_3 concentrations (Pryor et al., 2004; Saylor et al., 2010; Yao et al., 2013). Therefore, more efforts needed to be made to elucidate the contribution of vehicle-emitted NH_3 to the urban atmosphere.

Shanghai, like many other cities in eastern China, is suffering severe air pollution problems, such as high $\text{PM}_{2.5}$ concentrations and resulting poor visibility (Huang et al., 2013b; Huang et al., 2012). Although there are many studies aimed at understanding PM pollution, little is known about the characteristics of NH_3 in the largest city of China. In an effort to curb its severe air pollution, China recently launched an air pollution monitoring research program (known as the supersite program) in several major cities. In 2014, a new in situ atmospheric station equipped with state-of-the-art instruments was installed in the Shanghai region, allowing comprehensive characterization of $\text{PM}_{2.5}$ and associated precursor gases. Here seasonal trends, diurnal variations and pollution episodes retrieved from one year of real-time

measurement of NH_3 are presented and interpreted in order to explore the sources and parameters controlling the NH_3 concentrations across Shanghai. Meanwhile, an additional source-specific campaign was performed to examine the emission and transport of vehicle-emitted NH_3 from an urban heavily trafficked tunnel in Shanghai.

2 Methods

2.1 Long-term monitoring at Pudong supersite

In situ continuous observations of the chemical and optical properties of atmospheric aerosols and associated precursor gases were made on the rooftop (18 m above ground level) of the Pudong Environmental Monitoring Center (PEMC; 121.5446 °E, 31.2331 °N), 5 km east of the Shanghai urban center (the People's Square) (Figure 1). The site is located in a mixed-use urban area (office, commercial, residential and traffic) east of downtown Shanghai, with no obvious NH_3 point source within 5 km (Zou et al., 2015). As one of the state-controlled sites, Pudong (PD) supersite was designed by the Ministry of Environmental Protection of China and operated by the Shanghai Environmental Monitoring Center, being responsible for the release of hourly air quality data for PM_{10} , $\text{PM}_{2.5}$, and other criteria pollutants (CO , SO_2 , NO_x and O_3).

From 3 April 2014 to 2 April 2015, using a MARGA instrument (Measurement of Aerosols and Reactive Gases Analyzer, Metrohm Applikon B.V., NL), water-soluble gases (NH_3 , HNO_3 , HONO , HCl and SO_2) and $\text{PM}_{2.5}$ components (NO_3^- , Cl^- , SO_4^{2-} , Na^+ , NH_4^+ , K^+ , Mg^{2+} and Ca^{2+}) were measured with hourly temporal resolution. The MARGA removes soluble gases in a rotating, wet-walled denuder, while a steam-jet aerosol collector is used for fine particle collection. Meanwhile, aerosol light absorption coefficients (b_{abs}) were retrieved every 5 min from an AE31 Aethalometer using seven wavelengths (370, 470, 520, 590, 660, 880 and 950 nm) with a $\text{PM}_{2.5}$ cut-off inlet. Black carbon (BC) concentrations for the whole data set were calculated from the absorption coefficient at 880 nm. The measurement process was subjected to rigorous quality assurance and quality control procedures according to the Technical Guideline of Automatic Stations of Ambient Air Quality in Shanghai based on the national specification HJ/T193-2005. Meteorological parameters including temperature, relative humidity, and rainfall were monitored by an automatic meteorological station (Met One Instruments, US), which was co-located at the rooftop of the PD supersite.

To explore the comparability between on-line and off-line methods for NH_3 measurement, an Ogawa passive sampling device (PSD) was co-located with MARGA at PD to passively measure weekly ambient NH_3 concentration from May 2014 to June 2015. The Ogawa PSD is a double-sided passive sampler equipped with two 14 mm quartz filters (serving as duplicates) impregnated with phosphoric acid provided by the manufacturer. Following the manufacturer's protocols (<http://www.ogawausa.com>), exposed filter samples were soaked with 8 ml ultra-pure water (18.2 M Ω .cm) and analyzed by an ion chromatography system (883 Basic IC plus, Metrohm Co., Switzerland). The detection limit for NH_4^+ in the passive sampler extracts was 2.8 $\mu\text{g L}^{-1}$; this corresponds to an ambient NH_3 concentration detection limit of approximately 0.1 ppb for a 7-day sample. The NH_3 concentrations measured by the MARGA (ppb) were averaged over the same time period as the Ogawa PSDs (ppb). SI Figure S1 shows a good correlation ($y=0.82x+0.56$, $n=53$, $R^2=0.84$, $p<0.001$) between the two NH_3 measurement methods, validating the reliability of NH_3 data from the MARGA platform.

2.2 On-road measurement of NH_3 concentration in and out of a tunnel

To complement the information obtained from the main monitoring campaign described above, additional measurements of NH_3 concentration were performed at eight sites in and out the Handan tunnel from April 9 to May 21, 2014. The Handan tunnel is a 720 m long urban freeway in the northeast of Shanghai, separating the campus of Fudan University into two parts (Figure 9a). It contains an array of ventilation orifices in the middle section of the tunnel, 200 m in total. The tunnel has two traffic bores; each bore has a cross section of 70 m^2 and four lanes with typically 120000 vehicles (of which 85% of are light-duty vehicles) passing per day (Li, 2007). Driven by a group of high power fans, the average wind speed measured at the exit of the tunnel was approximately $5 \pm 1 \text{ m s}^{-1}$. The maximum vehicle speed limit in the tunnel is 80 km h^{-1} , with typical driving speeds of 50-60 km h^{-1} . Inside the northern bore of the tunnel, four sampling points were located at both ends of the tunnel (10 m from the exit and entrance of the tunnel, or T-d and T-a, for short) and the two ends of an array of ventilation orifices located in the middle section of the tunnel (Figure 9a; the site near the entrance and the exit named as T-b, and T-c for short, respectively). Outside the tunnel, a roadside transect involving four sites perpendicular to the tunnel was established, spanning the distance from 0 m ($\text{O}_{0\text{m}}$, for short), 20 m ($\text{O}_{20\text{m}}$), 150 m ($\text{O}_{150\text{m}}$), to 310 m ($\text{O}_{310\text{m}}$). Figure 9a shows the layout of the tunnel and the sampling points.

Using US EPA Method 207.1 (Determination of Ammonia Emissions from Stationary Sources), the NH_3 concentration at each site was measured. Briefly, for each sample, ambient air was pumped through two fritted glass bubblers (containing 10 ml 0.005 mol L^{-1} H_2SO_4 absorbing solution in each bubbler) for two hours at a flow rate of 1 L min^{-1} . These two bubblers were connected in series, and the NH_3 collection efficiency of the sampling trains was 95% or better (checked by using four bubblers in series in our pilot study, the collection efficiency = $100 \times (\text{the sum of the values of the first two bubblers}) / \text{the sum of the values of the four bubblers}$). Measurements were made during the morning (between 08:00 and 11:00 local time) and afternoon (between 14:00 and 19:00). Due to the proximity of the monitoring sites to the laboratory, all samples could be collected and analyzed by IC swiftly to avoid potential contamination, and field blanks were below the detection limit. Due to the dangers to personnel of sampling at the T-a, T-b and T-c sites, six samples were collected synchronously at these three sites. 19 paired samples were successfully collected and determined at the site of T-d, $\text{O}_{0\text{m}}$, $\text{O}_{20\text{m}}$, $\text{O}_{150\text{m}}$ and $\text{O}_{310\text{m}}$.

2.3 Planetary boundary layer height simulation

The Weather Research and Forecasting (WRF) model v3.5.1 (Skamarock et al., 2008) is used for simulating the height of planetary boundary layer. The WRF simulation was performed from a mother domain with a 45×45 km horizontal resolution over Asia, and nested down to a second domain of 15×15 km covering Eastern China, Korea and Japan, and further nested down to a third domain of 5×5 km covering the Yangtze Delta River region. Lambert conformal conic projection was used with true latitude limits of 4° and 44° and standing longitude of 115° . The coverage of three domains is shown in Supplement Fig. S4. We chose the RRTM longwave radiation scheme and the Dudhia shortwave radiation scheme. The Yonsei University scheme was used for the planetary boundary layer option. The WRF model configurations can be found elsewhere (Huang et al., 2013a). The National Centers for Environmental Prediction (NCEP) Final (FNL) Operational Global Analysis dataset (<http://rda.ucar.edu/datasets/ds083.2/>) with a horizontal resolution of a resolution of $1.0 \times 1.0^\circ$ are incorporated as initial and boundary conditions for the model. An one-way nested approach with four-dimensional data assimilation (FDDA) in WRF is applied. We have performed model evaluations of major meteorological parameters against the NCDC surface meteorological network (National Climate Data Center, <http://www7.ncdc.noaa.gov/CDO/cdo>) within the YRD region (red dots marked in Supplement Fig. S4). The evaluation results of

surface wind speed, temperature, and humidity are shown in Supplement Table S2. It could be seen that these meteorological parameters are within the benchmarks during most of the months, suggesting our WRF modeling results are reliable. A Meteorology/Chemistry Interface Processor (MCIP) (Otte and Pleim, 2010) v4.1 is used to post-process the WRF results by outputting the atmospheric height of the planetary boundary layer field, one of the standard MCIP outputs. The simulation period is consistent with the observation, i.e. from April, 2014 to April, 2015. In this study, PBLH derived from the third domain is used. Additionally, the planetary boundary layer depths at 3-hour resolution were obtained from the US National Oceanic and Atmospheric Administration (NOAA) READY archived Global Data Assimilation System (GDAS) meteorological data ($1^{\circ} \times 1^{\circ}$) based on Coordinated Universal Time (UTC). All UTC values are converted to local time (UTC + 8).

2.4 Potential source contribution analysis

24 h back trajectories arriving at the PD supersite at a height of 500 m were calculated at 1 h time intervals for each of the four seasons using NOAA Hybrid Single-Particle Lagrangian Integrated Trajectory (HYSPLIT) model with GDAS one degree archive meteorological data (Draxler and Rolph, 2015). An in-depth back trajectory analysis, the potential source contribution function (PSCF), is useful for identifying the possible geographic origin of emission sources; this method calculates the ratio of the number of points with concentration higher than a threshold value (m_{ij}) to the total number of points (n_{ij}) in the ij th grid cell. Higher PSCF values indicate higher potential source contributions to the receptor site. In this study, the domain for the PSCF was set within the range of (26-42°N, 112.5-125.5°E) in $0.1^{\circ} \times 0.1^{\circ}$ grid cells. The 75th percentile for CO and NH₃ during the four seasons was used as the threshold value m_{ij} . To reduce the uncertainties of m_{ij}/n_{ij} for those grid cells with a limited number of points, a weighting function recommended by (Polissar et al., 2001) was applied to the PSCF in each season. Visualizations of the PSCF were mapped using ArcMap 10.2.

3 Results and discussion

3.1 Temporal evolution of NH₃ concentrations

The temporal patterns of hourly gaseous NH₃ concentrations determined by the MARGA at the Pudong supersite are reported in Figure 2. Summary statistics for NH₃ concentrations ($\mu\text{g m}^{-3}$) during April 3, 2014-April 2, 2015 are shown in Table 1. Using a variety of chemical,

physical and optical techniques, numerous studies have examined ambient NH_3 concentrations over the last three decades; however, few of them were conducted in urban areas. As a comparison, we compiled previous work related to the measurement of urban NH_3 concentrations in Table 2.

The one year dataset ($n=8441$; data availability 96.4%) in the current study represents one of the longest on-line continuous measurement series of atmospheric NH_3 in China. During the study period, the NH_3 concentrations varied between 0.1 and $39.2 \mu\text{g m}^{-3}$, with an average ($\pm 1\sigma$) of $5.5 \pm 3.9 \mu\text{g m}^{-3}$. Domestically, the annual average NH_3 concentrations in Beijing and Xi'an were much higher than in Shanghai (see Table 2). This might be expected since Beijing and Xi'an are located in the North China Plain (NCP) and the Guanzhong Plain (GZP), respectively. The NCP and GZP are two of the most intensive agricultural production regions in China. Moreover, the NH_3 loss from soil increases with an increase in soil pH value (Ju et al., 2009). Shanghai and its surrounding regions are dominated by the acid soils of paddy fields (Figure 1) (Zhao et al., 2009), while Beijing and Xi'an are dominated by the alkaline soils of dry land (Wei et al., 2013). Internationally, the NH_3 concentration level in Shanghai was similar to observations from cities in developed and middle-income countries, but much lower than those cities in emerging countries. This is particularly true when comparing with cities in South Asia (e.g., Delhi in India and Lahore in Pakistan), where there is a lack of basic sanitation facilities (e.g., public flush toilets) and significant animal populations (such as cow) coexist with people in urban areas. The higher NH_3 concentrations measured at surface sites in South Asia are consistent with spatial patterns from recent satellite remote sensing observations (Clarisse et al., 2009; Van Damme et al., 2014).

The variations of NH_3 in spring and summer were generally consistent with fluctuations of temperature (Figure 2a). In winter, their correlations turned to be much weaker (Fig. 4a). While in autumn, no significant correlation between temperature and NH_3 was observed (Fig. 4a). Monthly, from March to September, the NH_3 concentration first increased steadily, with the highest value in July, then decreased gradually, along with falling temperature (Figure 2c). In summer (June to August), high temperatures favor NH_3 volatilization from urea and other N fertilizers applied to croplands (Fu et al., 2013; Huang et al., 2011; Ianniello et al., 2010; Meng et al., 2011). High temperatures in summer also favor NH_3 emission from other sources, such as animal housing, landfills, laystalls and pit latrines, animal manure, natural and fertilized soils, vegetation, and municipal solid waste (Fu et al., 2013; Huang et al., 2011).

Moreover, given that the equilibrium between ammonium nitrate particles and gaseous ammonia and nitric acid favors the gas phase compounds at higher temperature, warmer summer conditions promote dissociation of ammonium nitrate particles, shifting the ammonium/ammonia partitioning toward the gas phase (Behera et al., 2013). In this study, the average NH_3 concentration in summer ($7.3 \pm 4.9 \mu\text{g m}^{-3}$; $n=2181$) was $2.4 \mu\text{g m}^{-3}$ or 41% higher than the average of other seasons. The gap between summer and winter in Shanghai was similar to New York, but generally much lower than many other cities. Taking Beijing for example, according to Ianniello et al. (2010), the NH_3 concentration in summer was 460% higher than in winter; this figure was 320% in Xi'an between 2006 and 2007 (Cao et al., 2009). Smaller seasonal temperature differences and less agricultural activity in Shanghai could be the contributing factors.

Based on the “bottom-up” methodologies, previous emission inventories indicate that livestock feeding and N-fertilizer application contribute around 50% (48%-54.9%) and 35% (33.4%-40%) of the total NH_3 emissions in the Yangtze River delta region (YRD for short, including Shanghai as well as 24 cities in the provinces of Jiangsu and Zhejiang), respectively (Fu et al., 2013; Huang et al., 2011; Huang et al., 2012). Agricultural production is also the dominant source of NH_3 emissions in most other regions worldwide (Bouwman et al., 1997; Olivier et al., 1998; Reis et al., 2009). However, performed at an urban level, many studies in Table 2 concluded that the concentrations and evolution of ambient NH_3 in urban areas were influenced by traffic emissions. As one of the world's largest megacities, Shanghai might expect contributions of vehicle-emitted NH_3 as well. NH_3 concentrations in the atmosphere, however, are also sensitive to other important factors such as changes in temperature, wind speed or direction, and boundary layer depth; other influential factors might include local or regional NH_3 emissions, dry and wet deposition, and gas-to-particle partitioning. The relative importance of such factors in controlling ambient NH_3 concentration may vary seasonally. For example, the highest and lowest daily NH_3 concentrations in Shanghai were observed on 10-11 July 2014 ($23.4 \pm 6.7 \mu\text{g m}^{-3}$) and 10-11 March 2015 ($0.5 \pm 0.4 \mu\text{g m}^{-3}$), respectively. For the two periods, there was no significant difference between them in terms of wind speed and planetary boundary layer height (the relative humidity data in March period was missed). Although 19.6 mm of rainfall in the July period would be expected to lower NH_3 levels, the temperature on this high concentration date (28.4°C) was much higher than on the low concentration March date (4.7°C). Over a longer time frame, even though rainfall in summer

was around twice the amount of rainfall in other seasons, other factors such as greater NH_3 emissions at higher temperature outweigh the wet scavenging effects of rainfall yielding higher summertime NH_3 concentrations. High NH_3 concentration episodes during burning of agricultural wheat residues, indicated by a strong and synchronous rise of trace aerosols from biomass burning (e.g., K^+ and BC), were also evident in late spring (Figure 2b). The evolution of this pollution episode induced by biomass burning and its influence on the air quality of Shanghai has been examined in our recent paper (Zou et al., 2015).

3.2 Effects of meteorological parameters

In the following, we will examine the (synergistic) effects of various meteorological parameters on measured NH_3 concentrations in Shanghai, because these factors may mask the effect of vehicular emissions on the measured NH_3 concentrations. Summary statistics for meteorological parameters during April 3, 2014-April 2, 2015 are shown in Table 3.

Planetary boundary layer (PBL) height plays a vital role in determining the vertical dispersion of air pollutants that are emitted from the Earth surface. Decreasing height of PBL can normally hold the pollutants within the shallow surface layer so as to suppress the vertical atmospheric dilution. In many previous studies, as described above, the NH_3 concentrations in winter were much lower than those in summer. However, the NH_3 concentrations observed here in Shanghai during winter are relatively high. One may argue that weaker vertical mixing and shallow PBL layers in winter could trap NH_3 and contribute to elevated concentrations. In Figure 3a, although the simulated average PBL height in winter is the lowest during our study period, there is no significant difference among different seasons. In Figure 3b, the average PBL height in winter is even higher than that in spring and summer. Therefore, a relatively high NH_3 concentration in winter at PD cannot be fully explained by the strength of vertical mixing or PBL height in this study.

Figure 4a suggests that temperature (T) is an important driver of the increase of NH_3 concentration in spring. No clear relationship is seen for other seasons. As the transitional period between winter and summer, springtime in Shanghai has the highest standard deviation of temperature during our study period (Table 3). Additionally, spring is known as the sowing season in South China, with the greatest application of N-containing fertilizers (mainly in the form of urea) of the year. Warming temperature tends to increase the rate of urea hydrolysis and ammonium conversion to NH_3 , and therefore volatilization. For example, an increase in

temperature from 7.2 °C to 15.6 °C can double volatilization loss when moisture content is kept the same (Ernst and Massey, 1960). For relative humidity (RH), there is no clear evidence to suggest RH as an important factor controlling the dynamics of NH₃ concentrations in any of the seasons (Figure 4b). Figure S2 shows the RH and *T* dependent distributions of NH₃ concentration for each season. Given the generally poor relationship between the NH₃ concentration and *T* and RH as discussed above, NH₃ concentrations have no clear dependence on *T* and RH seasonally.

In Figures 5a and b the distribution of hourly average wind speeds was calculated for values between 0 m s⁻¹ and 4.0 m s⁻¹ (99.5% of occurrence). Figure 5a shows that there is a highly significant relationship between WS and NH₃ concentration ($R^2=0.91$, $p<0.001$). The highest average NH₃ concentrations were measured under the lowest wind speeds and the lowest concentrations were measured at the highest wind speeds. There is no clear relationship between wind frequency (the number of wind occurrence) and average NH₃ concentration or WS during the study period (Figure 5c). Figure S3 shows WS/WD dependence of NH₃ concentrations in different seasons. The distribution of NH₃ concentration showed an obvious concentration gradient as a function of WS. Seasonally, there are different preferential wind directions for the highest NH₃ concentration values. Generally, an overwhelming higher *T* in summer tends to greatly enhance the contribution of temperature-dependent emissions to the urban NH₃ budget from agricultural areas. And the nearby rural areas around Pudong supersite are in the direction of Southeast (Nanhui) and Northeast (Chongming) (Figure 6d). However, it is unexpected that in Shanghai, almost all high NH₃ concentration values in summer are concentrated in the direction of South-Southwest-West (SI Figure S3b), which strongly indicates that the urban area is one of the most important NH₃ emission regions in Shanghai.

Figures 6a and 6b show the RH and *T* dependent distributions of NH₃ and WS for the entire study period, respectively. Although the distribution of higher NH₃ favors the condition of high *T* (>25 °C), low RH (<60%) and low WS (<1.2 m s⁻¹), Figure 6a shows that there is no obvious concentration gradient as a function of RH and *T* (Note that in SI Figure S2d, higher NH₃ concentrations in winter tend to occur at higher *T* for a given RH range of 60% to 80%). This can be explained by the dominance of low WS (often lower than 1.2 m s⁻¹) during east-southeast and west-northwest wind directions associated with intense local sources for NH₃

within the city (Figure 6c). In brief, our results suggest that there are some temperature-independent and important NH_3 sources in the urban area of Shanghai.

3.3 NH_3 diurnal profiles and insight into sources

Hourly observations over long-term periods offer a unique opportunity to provide robust diurnal profiles for each season. Figure 7 shows the average diurnal profiles of NH_3 and CO concentrations across seasons. Historically, CO emissions in Shanghai and its surrounding YRD region mainly came from iron and steel manufacturing and on-road vehicles, which contributed 34% and 30% of the total, respectively in 2007 (Huang et al., 2011). Due to changing economic activity, emission sources of air pollutants in China are changing rapidly. For example, over the past several years, China has implemented a portfolio of plans to phase out its old-fashioned and small steel mills, and raise standards for industrial pollutant emissions (Chang et al., 2012). In contrast, China continuously experienced double digit growth in terms of auto sales during the same period, and became the world's largest automobile market since 2009 (Chang, 2014). Consequently, on-road traffic has overtaken industrial sources as the dominant source of CO emissions in Eastern China (Zhao et al., 2012). In Figure 7, CO shows a well-marked bimodal diurnal profile, with maxima in the morning (starting at 05:00 local time) and the evening (starting at 16:00), consistent with the variation of traffic flow in Shanghai (Liu et al., 2012). Therefore, CO variation can be utilized as a robust indicator of vehicle emissions. NH_3 also displays a clear bimodal profile during all four seasons, similar to the CO diurnal profile, suggesting a significant influence of on-road traffic (with daily commuting) on ambient NH_3 concentrations in the urban environment of Shanghai. We also notice that pools of surface water (i.e. dew or fog), which form on nights that have a high RH, can act as NH_x reservoirs that release NH_3 upon evaporation in the mid-morning, particularly in spring seasons.

Interestingly however, NH_3 shows different degrees of positive relationship with CO as a function of season (Figure 8b). Specifically, during summertime, NH_3 displays a significant relationship with CO ($R^2=0.48$, $p<0.001$), while this positive relationship is not observed during the winter season, when heavy traffic volume also occurs. As discussed above, the seasonal variation of NH_3 concentration in Shanghai during our study period was quite flat. The seasonal average CO concentrations at PD were 0.71, 0.61, 0.58, and 1.1 ppmv in spring, summer, autumn, and winter, respectively. And the CO level in wintertime was higher than

other seasons. Moreover, Figure 8c suggests that for all seasons, the source region of NH₃ in Shanghai is local-dominated. However, the atmospheric lifetime of CO is much longer than that of NH₃ (typically several hours depending on meteorology) (Asman et al., 1998). PSCF analysis for CO in winter suggests important contributions from north of Shanghai (Figure 8a), a region that does not appear as important as a NH₃ source (Figure 8c). Consequently, elevated regional background levels of CO from long-range transport appear to yield a poorer relationship between NH₃ and CO in wintertime (Figure 8b).

3.4 The emission and transport of vehicle-sourced NH₃

SI Table S1 summarizes statistics of the NH₃ concentrations ($\mu\text{g m}^{-3}$) measured at each sampling point in and out of the Handan tunnel, which have been also been visualized in Figure 9b. As expected, the highest average NH₃ concentration occurred at the exit of the tunnel (T-d). Although NH₃ concentration varied temporally, throughout the two months of observations, a large spatial gradient in NH₃ concentration at near-road sites was present in every sampling event, suggesting that an intensive NH₃ source from on-road traffic (not meteorological parameters) is the leading factor in governing the variation of ambient NH₃ concentration in a road-side environment. The NH₃ concentrations in the tunnel were increased with distance from the entrance of the tunnel (T-a). The NH₃ concentration at T-d ($64.9 \pm 11.5 \mu\text{g m}^{-3}$) was over 5 times that at T-a ($12.6 \pm 3.3 \mu\text{g m}^{-3}$). Moreover, the lowest NH₃ concentration value obtained at T-d ($47.0 \mu\text{g m}^{-3}$) was still nearly $10 \mu\text{g m}^{-3}$ or 20% higher than the highest value of other sites (SI Table S1). These observations provide compelling evidence that on-road traffic is an important emission source of NH₃ in the urban atmosphere. Given that there is a significant loss of vehicle exhaust from the tunnel through an array of ventilation orifices in the middle section of the tunnel, the NH₃ concentration at T-b ($29.2 \pm 6.6 \mu\text{g m}^{-3}$) was close to that at T-c ($31.5 \pm 5.9 \mu\text{g m}^{-3}$). If we taking into account of the **Physical Distance** (PD; 300 m) and the **NH₃ Concentration Gap** (CG; $33.4 \pm 11.5 \mu\text{g m}^{-3}$) between T-c and T-d, the **Cross Section** of tunnel bore (CS; 70 m^3), the average **Wind Speed** (WS; 5 m s^{-1}) and **Traffic Flow** (TF; $120000 \text{ vehicles day}^{-1}$), we can obtain an approximate mileage-based NH₃ **Emission Factor** (EF) of $28 \pm 5 \text{ mg km}^{-1}$ for a single vehicle using the following equation:

$$EF = \frac{CG \times CS \times WS \times 86400}{TF \times PD} \quad (1)$$

where 86400 is the number of seconds in a day. This NH_3 emission factor was similar to that observed for the Gurbrist tunnel in Switzerland ($31 \pm 4 \text{ mg km}^{-1}$) (Emmenegger et al., 2004) and the Caldecott tunnel in California ($49 \pm 3 \text{ mg km}^{-1}$) (Kean et al., 2000), while much lower than that recently measured in Guangzhou, China ($230 \pm 14 \text{ mg km}^{-1}$) (Liu et al., 2014). Based on the emission factor we developed, a population of 3.04 million vehicles (average mileage of 15000 km yr^{-1}) in Shanghai would produce around 1300 t NH_3 in 2014. This is very close to the “bottom-up” emission inventory in Shanghai for 2010 (1581.1 t) (Chang, 2014). Previous emission inventories in Shanghai (e.g., Huang et al. (2011) and Fu et al. (2012)) made a significant underestimation of the NH_3 emissions from city areas. When compared with the NH_3 emissions from city area, the contribution of on-road traffic can reach 12% of the total NH_3 emissions in Shanghai city areas (10742 t) (Chang, 2014). Moreover, model results have shown that over half of agricultural NH_3 emissions would be deposited downwind of its source within 10 km depending on local meteorological conditions (Asman et al., 1998). Therefore, the relative contribution of NH_3 emissions from on-road traffic to urban PM pollution could be higher than the share of its mass contribution. Given that precisely estimating the EF of NH_3 from on-road traffic is beyond the scope of this paper, more research is needed to pinpoint this parameter in order to accurately quantify the amount of NH_3 emissions from vehicles.

From the tunnel exit to the open environment, the average NH_3 concentration at T-d ($64.9 \pm 11.5 \text{ } \mu\text{g m}^{-3}$) was 11 times more than that at $\text{O}_{310\text{m}}$ ($5.6 \pm 2.5 \text{ } \mu\text{g m}^{-3}$), and a general negative relationship was found between distance and ambient NH_3 concentration. Over the total measured distance, the maximum percent decrease was observed between the sites of T-d and $\text{O}_{0\text{m}}$ (50 m apart), indicating a rapid dispersion of vehicle-emitted NH_3 from the road tunnel. Still, Figure 9c clearly shows that 64% (48%) of the NH_3 concentration we observed at the site of $\text{O}_{0\text{m}}$ ($\text{O}_{20\text{m}}$) can be explained by the simultaneous measurements of NH_3 concentration at T-d. No significant decrease in the gradients of NH_3 concentration was observed between the sites of $\text{O}_{150\text{m}}$ ($5.9 \pm 2.5 \text{ } \mu\text{g m}^{-3}$; $n=6$) and $\text{O}_{310\text{m}}$ ($5.6 \pm 2.5 \text{ } \mu\text{g m}^{-3}$; $n=6$), suggesting that the strongest impact of NH_3 emission and transport from local traffic flow on ambient NH_3 concentrations in the Shanghai urban area lies within 150 m distance.

4 Conclusions and outlook

This study linked a long-term and near real-time measurement of NH_3 at one of China's flagship supersites with a vehicle source-specific campaign performed in and out of a major freeway tunnel in Shanghai. The conclusions are shown as below:

- The average NH_3 concentration ($\text{mean} \pm 1\sigma$) between April, 2014 and April, 2015 was $5.5 \pm 3.9 \mu\text{g m}^{-3}$. Seasonal NH_3 concentration levels varied in the following sequence: summer ($7.3 \pm 4.9 \mu\text{g m}^{-3}$) > spring ($5.1 \pm 3.8 \mu\text{g m}^{-3}$) \approx winter ($5.0 \pm 3.4 \mu\text{g m}^{-3}$) > fall ($4.5 \pm 2.3 \mu\text{g m}^{-3}$).
- During spring, ambient NH_3 concentrations appeared to be influenced to some extent by temperature-dependent emissions, likely from agricultural activities including crop fertilization. No such relationship was apparent during other seasons. Measured NH_3 concentrations were highly dependent on wind speed, while mixing height of planetary boundary layer and relative humidity were not the main factors influencing seasonal NH_3 concentrations.
- The diurnal profile of NH_3 concentrations showed a typical bimodal cycle during four seasons, with maxima in the morning and the evening rush hours, suggesting a persistent influence of on-road traffic (with daily commuting) on ambient NH_3 levels in Shanghai.
- The NH_3 concentration in the exit of the Handan tunnel ($64.9 \pm 11.5 \mu\text{g m}^{-3}$) was over 5 and 11 times higher than that in the tunnel entrance ($12.6 \pm 3.3 \mu\text{g m}^{-3}$) and the ambient air ($5.6 \pm 2.5 \mu\text{g m}^{-3}$), respectively, providing further compelling evidence that on-road traffic is an important NH_3 source. 1300 t vehicle-emitted NH_3 in 2014 was calculated based on a mileage-based NH_3 emission factor of $28 \pm 5 \text{ mg km}^{-1}$ we developed.
- A negative relationship was found between the distance and ambient NH_3 concentration in our near-road gradient experiment. Up to 64% of ambient NH_3 concentration out of the tunnel can be explained by the vehicle-emitted NH_3 from the tunnel.

Unlike NH_3 emissions in agricultural areas, the NH_3 emissions in urban areas originate from a variety of stationary sources (industrial coal/oil/gas combustion, wastewater, landfill, compost and incineration), mobile sources and area sources (e.g., humans, green land, domestic fuel combustion). As a start, our study is far from fully elucidating the complex origins of urban

NH₃ in Shanghai. Vehicle-emitted NH₃, while important, is likely not the only major source of NH₃. Additional useful investigative steps could include:

- Using isotopes as a source apportionment tool. Isotopic techniques have been proven to be useful tools for sources apportionment of gases and PM. Although the $\delta^{15}\text{N}$ values of NH₄⁺ in rainwater and aerosols have been examined (Xiao et al., 2015; Xiao and Liu, 2002; Xiao et al., 2012), atmospheric NH₃ has received much less attention. According to Felix et al., (2013), NH₃ emitted from volatilized sources has relatively low $\delta^{15}\text{N}$ values, allowing them to be distinctly differentiated from NH₃ emitted from fuel-related sources (e.g., on-road traffic) that are characterized by relatively high $\delta^{15}\text{N}$ values.
- Using chemical transport modeling (CTM) as a cost-effective analysis tool. CTM has the potential to capture the complex atmospheric behavior of NH₃. Moreover, NH₃ emission reduction targets are represented as constraints in the optimization problem, and have a major influence on overall costs of a cost-effective solution and their distribution across different sources and economic sectors. Through sensitivity analyses of specific emission source or assuming possible emission control scenarios, CTM can contribute to the setting of effective emission reduction strategies to achieve cost-effective improvements in air quality.

Acknowledgements

Special thanks go to Tony Dore (CEH, UK), Yunting Fang (CAS, CN) and Fujiang Wang (Fudan, CN) for their insightful comments. This work was supported financially by the National Natural Science Foundation of China (Grant Nos. 21377029, 21277030 and 41405115). We also acknowledge the Qingyue Open Environmental Data Centre (data.epmap.org). Yunhua Chang acknowledges the support of Gao Tingyao scholarship. Kan Huang acknowledges the award from the 1000 Plan Program for Young Talents. The computational resources used in this work are supported by the University of Tennessee and Oak Ridge National Laboratory Joint Institute for Computational Sciences (<http://www.jics.tennessee.edu>). The authors declare no competing financial interest.

References

- Aneja, V. P., Chauhan, J. P., and Walker, J. T.: Characterization of atmospheric ammonia emissions from swine waste storage and treatment lagoons, *J. Geophys. Res.*, 105(D9), 11535-11545, doi: 10.1029/2000JD900066, 2003.
- Asman, W. A., Sutton, M. A., and Schjørring, J. K.: Ammonia: emission, atmospheric transport and deposition, *New Phytol.*, 139(1), 27-48, doi: 10.1046/j.1469-8137.1998.00180.x, 1998.
- Bari, A., Ferraro, V., Wilson, L. R., Luttinger, D., and Husain, L.: Measurements of gaseous HONO, HNO₃, SO₂, HCl, NH₃, particulate sulfate and PM_{2.5} in New York, NY, *Atmos. Environ.*, 37(20), 2825-2835, doi: 10.1016/S1352-2310(03)00199-7, 2003.
- Behera, S. N., Sharma, M., Aneja, V. P., and Balasubramanian, R.: Ammonia in the atmosphere: a review on emission sources, atmospheric chemistry and deposition on terrestrial bodies, *Environ. Sci. Pollut. R. Int.*, 20(11), 8092-8131, doi: 10.1007/s11356-013-2051-9, 2013.
- Bettez, N. D., Marino, R., Howarth, R. W., and Davidson, E. A.: Roads as nitrogen deposition hot spots, *Biogeochem.*, 114(1-3), 149-163, doi: 10.1007/s10533-013-9847-z, 2013.
- Bishop, G. A., and Stedman, D. H.: Reactive nitrogen species emission trends in three light-/medium-duty United States fleets, *Environ. Sci. Technol.*, 49(18), 11234-11240, doi: 10.1021/acs.est.5b02392, 2015.
- Biswas, K. F., Ghauri, B. M., and Husain, L.: Gaseous and aerosol pollutants during fog and clear episodes in South Asian urban atmosphere, *Atmos. Environ.*, 42(33), 7775-7785, doi: 10.1016/j.atmosenv.2008.04.056, 2008.
- Blanchard, C. L., Roth, P. M., Tanenbaum, S. J., Ziman, S. D., and Seinfeld, J. H.: The use of ambient measurements to identify which precursor species limit aerosol nitrate formation, *J. Air Waste Manage. Assoc.*, 50(12), 2073-2084, doi: 10.1080/10473289.2000.10464239, 2000.
- Bouwman, A. F., Lee, D. S., Asman, W. A. H., Dentener, F. J., Van Der Hoek, K. W., and Olivier, J. G. J.: A global high-resolution emission inventory for ammonia, *Global Biogeochem. Cy.*, 11(4), 561-587, doi: 10.1029/97GB02266, 1997.
- Brito, J., Rizzo, L. V., Herckes, P., Vasconcellos, P. C., Caumo, S. E. S., Fornaro, A., Ynoue, R. Y., and Andrade, M. F.: Physical–chemical characterisation of the particulate matter inside two road tunnels in the São Paulo Metropolitan Area, *Atmos. Chem. Phys.*, 13(24), 12199-12213, doi: 10.5194/acp-13-12199-2013, 2013.

552 Brook, J. R., Wiebe, A. H., Woodhouse, S. A., Audette, C. V., Dann, T. F., Callaghan, S.,
553 Piechowski, M., Dabek-Zlotorzynska, E., and Dlouhy, J. F.: Temporal and spatial
554 relationships in fine particle strong acidity, sulphate, PM₁₀, and PM_{2.5} across multiple
555 Canadian locations, *Atmos. Environ.*, 31(24), 4223-4236, doi: 10.1016/S1352-
556 2310(97)00248-3, 1997.

557 Broxton, P. D., Zeng, X., Sulla-Menashe, D., and Troch, P. A.: A global land cover
558 climatology using MODIS data, *J. Appl. Meteorol. Clim.*, 53(6), 1593-1605,
559 doi: 10.1175/JAMC-D-13-0270.1, 2014.

560 Cadle, S. H., Countess, R. J., and Kelly, N. A.: Nitric acid and ammonia in urban and rural
561 locations, *Atmos. Environ.*, 16(10), 2501-2506, doi: 10.1016/0004-6981(82)90141-X, 1982.

562 Cao, J. J., Zhang, T., Chow, J. C., Watson, J. G., Wu, F., and Li, H.: Characterization of
563 atmospheric ammonia over Xi'an, China, *Aerosol Air Qual. Res.*, 9(2), 277-289, doi:
564 10.4209/aaqr.2008.10.0043, 2009.

565 Cape, J. N., Tang, Y. S., Van Dijk, N., Love, L., Sutton, M. A., and Palmer, S. C. F.:
566 Concentrations of ammonia and nitrogen dioxide at roadside verges, and their contribution
567 to nitrogen deposition, *Environ. Pollut.*, 132(3), 469-478, doi:
568 10.1016/j.envpol.2004.05.009, 2004.

569 Chang, Y. H.: Non-agricultural ammonia emissions in urban China, *Atmos. Chem. Phys.*
570 *Discuss.*, 14(6), 8495-8531, doi: 10.5194/acpd-14-8495-2014, 2014.

571 Chang, Y. H., Liu, X., Dore, A. J., and Li, K.: Stemming PM_{2.5} pollution in China: Re-
572 evaluating the role of ammonia, aviation and non-exhaust road traffic emissions, *Environ.*
573 *Sci. Technol.*, 46(24), 13035-13036, doi: 10.1021/es304806k, 2012.

574 Clarisse, L., Clerbaux, C., Dentener, F., Hurtmans, D., and Coheur, P. F.: Global ammonia
575 distribution derived from infrared satellite observations, *Nature Geos.*, 2(7), 479-483, doi:
576 10.1038/ngeo551, 2009.

577 Draxler, R. R., and Rolph, G. D.: HYSPLIT (HYbrid Single-Particle Lagrangian Integrated
578 Trajectory) Model access via NOAA ARL READY Website
579 (<http://ready.arl.noaa.gov/HYSPLIT.php>). Rep., NOAA Air Resources Laboratory, Silver
580 Spring, MD.

581 Durbin, T. D., Wilson, R. D., Norbeck, J. M., Miller, J. W., Huai, T., and Rhee, S. H.:
582 Estimates of the emission rates of ammonia from light-duty vehicles using standard chassis
583 dynamometer test cycles, *Atmos. Environ.*, 36(9), 1475-1482, doi: 10.1016/S1352-
584 2310(01)00583-0, 2002.

585 Emmenegger, L., Mohn, J., Sigrist, M., Marinov, D., Steinemann, U., Zumsteg, F., and Meier,
586 M.: Measurement of ammonia emissions using various techniques in a comparative tunnel
587 study, *Int. J. Environ. Pollut.*, 22(3), 326-341, doi: 10.1504/IJEP.2004.005547, 2004.

588 Ernst, J. W., and Massey, H. F.: The effects of several factors on volatilization of ammonia
589 formed from urea in the soil, *Soil Sci. Soc. Proc.*, 24, 87-90, doi:
590 10.2136/sssaj1960.03615995002400020007x, 1960.

591 Felix, J. D., Elliott, E. M., Gish, T. J., Maghirang, R., Cambal, L., and Clougherty, J.:
592 Examining the transport of ammonia emissions across landscapes using nitrogen isotope
593 ratios, *Atmos. Environ.*, 95, 563-570, doi: 10.1016/j.atmosenv.2014.06.061, 2014.

594 Felix, J. D., Elliott, E. M., Gish, T. J., McConnell, L. L., and Shaw, S. L.: Characterizing the
595 isotopic composition of atmospheric ammonia emission sources using passive samplers and
596 a combined oxidation-bacterial denitrifier approach, *Rapid Commun. Mass Sp.*, 27(20),
597 2239-2246, doi: 10.1002/rcm.6679, 2013.

598 Fountoukis, C., Nenes, A., Sullivan, A., Weber, R., Reken, T. V., Fischer, M., Matias, E.,
599 Moya, M., Farmer, D., and Cohen, R. C.: Thermodynamic characterization of Mexico City
600 aerosol during MILAGRO 2006, *Atmos. Chem. Phys.*, 9(6), 2141-2156, doi: 10.5194/acp-
601 9-2141-2009, 2009.

602 Fraser, M. P., and Cass, G. R.: Detection of excess ammonia emissions from in-use vehicles
603 and the implications for fine particle control, *Environ. Sci. Technol.*, 32(8), 1053-1057, doi:
604 10.1021/es970382h, 1998.

605 Fu, X., Wang, S., Zhao, B., Xing, J., Cheng, Z., Liu, H., and Hao, J.: Emission inventory of
606 primary pollutants and chemical speciation in 2010 for the Yangtze River Delta region,
607 China, *Atmos. Environ.*, 70, 39-50, doi: 10.1016/j.atmosenv.2012.12.034, 2013.

608 Gay, S. W., Schmidt, D. R., Clanton, C. J., Janni, K. A., Jacobson, L. D., and Weisberg, S.:
609 Odor, total reduced sulfur, and ammonia emissions from animal housing facilities and
610 manure storage units in Minnesota, *Appl. Eng. Agric.*, 19(3), 347-360, doi:
611 10.13031/2013.13663, 2003.

612 Giroux, M., Esclassan, J., Arnaud, C., and Chalé J. J.: Analysis of levels of nitrates and
613 derivatives of ammonia in an urban atmosphere, *Sci. Total Environ.*, 196(3), 247-254, doi:
614 10.1016/S0048-9697(96)05423-X, 1997.

615 Gong, L., Lewicki, R., Griffin, R. J., Flynn, J. H., and Lefer, B. L.: Atmospheric ammonia
616 measurements in Houston, TX using an external-cavity quantum cascade laser-based sensor,
617 *Atmos. Chem. Phys.*, 11(18), 9721-9733, doi: 10.5194/acp-11-9721-2011, 2011.

618 Gong, L., Lewicki, R., Griffin, R. J., Tittel, F. K., Lonsdale, C. R., Stevens, R. G., Pierce, J.,
619 Malloy, Q., Travis, S., Bobmanuel, L., Lefer, B., and Flynn, J. H.: Role of atmospheric
620 ammonia in particulate matter formation in Houston during summertime, *Atmos. Environ.*,
621 77, 893-900, doi: 10.1016/j.atmosenv.2013.04.079, 2013.

622 Heald, C. L., Collett Jr, J. L., Lee, T., Benedict, K. B., Schwandner, F. M., Li, Y., Clarisse, L.,
623 Hurtmans, D., Van Damme, M., Clerbaux, C., Coheur, P., and Pye, H. O. T.: Atmospheric
624 ammonia and particulate inorganic nitrogen over the United States, *Atmos. Chem. Phys.*,
625 12(21), 10295-10312, doi: 10.5194/acp-12-10295-2012, 2012.

626 Heeb, N. V., Saxer, C. J., Forss, A. M., and Brühlmann, S.: Trends of NO^- , NO_2^- , and NH_3 -
627 emissions from gasoline-fueled Euro-3-to Euro-4-passenger cars, *Atmos. Environ.*, 42(10),
628 2543-2554, doi: 10.1016/j.atmosenv.2007.12.008, 2008.

629 Heeb, N. V., Forss, A. M., Brühlmann, S., Lüscher, R., Saxer, C. J., and Hug, P.: Three-way
630 catalyst-induced formation of ammonia-velocity-and acceleration-dependent emission
631 factors, *Atmos. Environ.*, 40(31), 5986-5997, doi: 10.1016/j.atmosenv.2005.12.035, 2006.

632 Huai, T., Durbin, T. D., Younglove, T., Scora, G., Barth, M., and Norbeck, J. M.: Vehicle
633 specific power approach to estimating on-road NH_3 emissions from light-duty vehicles,
634 *Environ. Sci. Technol.*, 39(24), 9595-9600, doi: 10.1021/es050120c, 2005.

635 Huang, C., Chen, C. H., Li, L., Cheng, Z., Wang, H. L., Huang, H. Y., Streets, D., Wang, Y.,
636 Zhang, G., and Chen, Y. R.: Emission inventory of anthropogenic air pollutants and VOC
637 species in the Yangtze River Delta region, China, *Atmos. Chem. Phys.*, 11(9), 4105-4120,
638 doi: 10.5194/acp-11-4105-2011, 2011.

639 Huang, K., Zhuang, G., Lin, Y., Fu, J. S., Wang, Q., Liu, T., Zhang, R., Jiang, Y., and Deng,
640 C.: Typical types and formation mechanisms of haze in an eastern Asia megacity, Shanghai,
641 *Atmos. Chem. Phys.*, 12, 105-124, doi: 10.5194/acp-12-105-2012, 2012.

642 Huang, K., Fu, J. S., Hsu, N. C., Gao, Y., Dong, X., Tsay, S. C. and Lam, Y. F.: Impact
643 assessment of biomass burning on air quality in Southeast and East Asia during BASE-
644 ASIA, *Atmos. Environ.*, 78, 291-302, doi: 10.1016/j.atmosenv.2012.03.048, 2013a.

645 Huang, K., Zhuang, G., Lin, Y., Wang, Q., Fu, J. S., Fu, Q., Liu, T., and Deng, C.: How to
646 improve the air quality over megacities in China: Pollution characterization and source
647 analysis in Shanghai before, during, and after the 2010 World Expo, *Atmos. Chem. Phys.*,
648 13, 5927-5942, doi: 10.5194/acp-13-5927-2013, 2013b.

649 Huang, R. J., Zhang, Y., Bozzetti, C., Ho, K. F., Cao, J. J., Han, Y., Daellenbach, K., Slowik,
650 J., Platt, S., Canonaco, F., Zotter, P., Wolf, R., Pieber, S., Bruns, E., Crippa, M., Ciarelli, G.,

651 Piazzalunga, A., Schwilowski, M., Abbaszade, G., Schnelle-Kreis, J., Zimmermann, R., An,
 652 Z., Szidat, S., Baltensperger, U., El Haddad, L., and Prévôt, A. S.: High secondary aerosol
 653 contribution to particulate pollution during haze events in China, *Nature*, 514(7521), 218-
 654 222, doi: 10.1038/nature13774, 2014.

655 Ianniello, A., Spataro, F., Esposito, G., Allegrini, I., Rantica, E., Ancora, M. P., Hu, M., and
 656 Zhu, T.: Occurrence of gas phase ammonia in the area of Beijing (China), *Atmos. Chem.*
 657 *Phys.*, 10(19), 9487-9503, doi: 10.5194/acp-10-9487-2010, 2010.

658 Ju, X. T., Xing, G. X., Chen, X. P., Zhang, S. L., Zhang, L. J., Liu, X. J., Cui, Z. L., Yin, B.,
 659 Christie, P., Zhu, Z. L., and Zhang, F. S.: Reducing environmental risk by improving N
 660 management in intensive Chinese agricultural systems, *Proc. Natl. Acad. Sci. U.S.A.*,
 661 106(9), 3041-3046, doi: 10.1073/pnas.0813417106, 2009.

662 Kawashima, S., and Yonemura, S.: Measuring ammonia concentration over a grassland near
 663 livestock facilities using a semiconductor ammonia sensor, *Atmos. Environ.* 35(22), 3831-
 664 3839, doi: 10.1016/S1352-2310(01)00145-5, 2001.

665 Kean, A. J., Littlejohn, D., Ban-Weiss, G. A., Harley, R. A., Kirchstetter, T. W., and Lunden,
 666 M. M.: Trends in on-road vehicle emissions of ammonia, *Atmos. Environ.*, 43(8), 1565-
 667 1570, doi: 10.1016/j.atmosenv.2008.09.085, 2009.

668 Kean, A. J., Harley, R. A., Littlejohn, D., and Kendall, G. R.: On-road measurement of
 669 ammonia and other motor vehicle exhaust emissions, *Environ. Sci. Technol.*, 34(17), 3535-
 670 3539, doi: 10.1021/es991451q, 2000.

671 Lamarque, J. F., Bond, T. C., Eyring, V., Granier, C., Heil, A., Klimont, Z., Lee, D., Liousse,
 672 C., Mieville, A., Owen, B., Schultz, M., Schindell, D., Smith, S., Stehfest, E., Van
 673 Aardenne, J., Cooper, O., Kainuma, M., Mahowald, N., McConnell, J., Naik, V., Riahi, K.,
 674 and Van Vuuren, D. P.: Historical (1850-2000) gridded anthropogenic and biomass burning
 675 emissions of reactive gases and aerosols: methodology and application, *Atmos. Chem.*
 676 *Phys.*, 10(15), 7017-7039, doi: 10.5194/acp-10-7017-2010, 2010.

677 Leaderer, B. P., Naeher, L., Jankun, T., Balenger, K., Holford, T. R., Toth, C., Sullivan, J.,
 678 Wolfson, J. M., and Koutrakis P.: Indoor, outdoor, and regional summer and winter
 679 concentrations of PM₁₀, PM_{2.5}, SO₄²⁻, H⁺, NH₄⁺, NO₃⁻, NH₃, and nitrous acid in homes with
 680 and without kerosene space heaters, *Environ. Health Perspect.*, 107(3), 223-231, doi:
 681 10.1289/ehp.99107223, 1999.

682 Lee, H. S., Wadden, R. A., and Scheff, P. A.: Measurement and evaluation of acid air
683 pollutants in Chicago using an annular denuder system, *Atmos. Environ.*, 27(4), 543-553,
684 doi: 10.1016/0960-1686(93)90211-G, 1993.

685 Lee, H. S., Kang, C. M., Kang, B. W., and Kim, H. K.: Seasonal variations of acidic air
686 pollutants in Seoul, South Korea, *Atmos. Phys.*, 33(19), 3143-3152, doi: 10.1016/S1352-
687 2310(98)00382-3, 1999.

688 Li, K., Liu, X., Song, W., Chang, Y., Hu, Y., and Tian, C.: Atmospheric nitrogen deposition
689 at two sites in an arid environment of Central Asia, *Plos One*, 8(6), e67018, doi:
690 10.1371/journal.pone.0067018, 2013

691 Li, M.: Engineering design of the Handan Road tunnel in the Middle Ring Road, China Munic.
692 Eng. (A01), 34-38, 2007. (in Chinese with English abstract)

693 Li, Y. Q., Schwab, J. J., and Demerjian, K. L.: Measurements of ambient ammonia using a
694 tunable diode laser absorption spectrometer: Characteristics of ambient ammonia emissions
695 in an urban area of New York City, *J. Geophys. Res.*, 111(D10), D10S02, doi:
696 10.1029/2005JD006275, 2006.

697 Lin, J., Nielsen, C. P., Zhao, Y., Lei, Y., Liu, Y., and McElroy, M. B.: Recent changes in
698 particulate air pollution over China observed from space and the ground: effectiveness of
699 emission control, *Environ. Sci. Technol.*, 44(20), 7771-7776, doi: 10.1021/es101094t, 2010.

700 Lin, Y. C., Cheng, M. T., Ting, W. Y., and Yeh, C. R.: Characteristics of gaseous HNO₂,
701 HNO₃, NH₃ and particulate ammonium nitrate in an urban city of Central Taiwan, *Atmos.*
702 *Environ.*, 40(25), 4725-4733, doi: 10.1016/j.atmosenv.2006.04.037, 2006.

703 Liu, T., Wang, X., Wang, B., Ding, X., Deng, W., Lü S., and Zhang, Y.: Emission factor of
704 ammonia (NH₃) from on-road vehicles in China: Tunnel tests in urban Guangzhou, *Environ.*
705 *Res. Lett.*, 9(6), 064027, doi: 10.1088/1748-9326/9/6/064027, 2014.

706 Liu, Y., Wang, F. Xiao, Y., and Gao, S: Urban land uses and traffic ‘source-sink areas’:
707 Evidence from GPS-enabled taxi data in Shanghai, *Landscape Urban Plan.*, 106(1), 73-87,
708 doi: 10.1016/j.landurbplan.2012.02.012, 2012.

709 Livingston, C., Rieger, P., and Winer, A.: Ammonia emissions from a representative in-use
710 fleet of light and medium-duty vehicles in the California South Coast Air Basin, *Atmos.*
711 *Environ.*, 43(21), 3326-3333, doi: 10.1016/j.atmosenv.2009.04.009, 2009.

712 Ma, Z., Hu, X., Huang, L., Bi, J., and Liu, Y.: Estimating ground-level PM_{2.5} in China using
713 satellite remote sensing, *Environ. Sci. Technol.* 48(13), 7436-7444, doi:
714 10.1021/es5009399, 2014.

715 Ma, Z., Hu, X., Sayer, A. M., Levy, R., Zhang, Q., Xue, Y., Tong, S., Bi, J., Huang, L., and
 716 Liu, Y.: Satellite-based spatiotemporal trends in PM_{2.5} concentrations: China, 2004-2013,
 717 Environ. Health Perspect., accepted, doi: 10.1289/ehp.1409481, 2015.

718 Matsumoto, M., and Okita, T.: Long term measurements of atmospheric gaseous and aerosol
 719 species using an annular denuder system in Nara, Japan, Atmos. Environ., 32(8), 1419-
 720 1425, doi: 10.1016/S1352-2310(97)00270-7, 1998.

721 McCurdy, T., Zelenka, M. P., Lawrence, P. M., Houston, R. M., and Burton, R.: Acid
 722 aerosols in the Pittsburgh Metropolitan area, Atmos. Environ., 33(30), 5133-5145, doi:
 723 10.1016/S1352-2310(99)00119-3, 1999.

724 Meng, Z. Y., Lin, W. L., Jiang, X. M., Yan, P., Wang, Y., Zhang, Y. M., Jia, X., and Yu, X.
 725 L.: Characteristics of atmospheric ammonia over Beijing, China, Atmos. Chem. Phys.,
 726 11(12), 6139-6151, doi: 10.5194/acp-11-6139-2011, 2011.

727 Moeckli, M. A., Fierz, M., and Sigrist, M. W.: Emission factors for ethene and ammonia from
 728 a tunnel study with a photoacoustic trace gas detection system, Environ. Sci. Technol.,
 729 30(9), 2864-2867, doi: 10.1021/es960152n, 1996.

730 Mount, G. H., Rumburg, B., Havig, J., Lamb, B., Westberg, H., Yonge, D., Johnson, K., and
 731 Kincaid, R.: Measurement of atmospheric ammonia at a dairy using differential optical
 732 absorption spectroscopy in the mid-ultraviolet, Atmos. Environ., 36(11), 1799-1810, doi:
 733 10.1016/S1352-2310(02)00158-9, 2002.

734 Nowak, J. B., Neuman, J. A., Bahreini, R., Brock, C. A., Middlebrook, A. M., Wollny, A. G.,
 735 Holloway, J., Peischl, J., Ryerson, T., and Fehsenfeld, F. C.: Airborne observations of
 736 ammonia and ammonium nitrate formation over Houston, Texas, J. Geophys. Res.,
 737 115(D22), doi: 10.1029/2010JD014195, 2010.

738 Olivier, J. G. J., Bouwman, A. F., Van der Hoek, K. W., and Berdowski, J. J. M.: Global air
 739 emission inventories for anthropogenic sources of NO_x, NH₃ and N₂O in 1990, Environ.
 740 Pollut., 102(1), 135-148, doi: 10.1016/S0269-7491(98)80026-2, 1998.

741 Otte, T. L., and Pleim, J. E.: The Meteorology-Chemistry Interface Processor (MCIP) for the
 742 CMAQ modeling system: updates through MCIPv3.4.1, Geosci. Model Dev., 3(1), 243-256,
 743 doi:10.5194/gmd-3-243-2010, 2010.

744 Pandolfi, M., Amato, F., Reche, C., Alastuey, A., Otjes, R. P., Blom, M. J., and Querol, X.:
 745 Summer ammonia measurements in a densely populated Mediterranean city, Atmos. Chem.
 746 Phys., 12(16), 7557-7575, doi: 10.5194/acp-12-7557-2012, 2012.

747 Parmar, R. S., Satsangi, G. S., Lakhani, A., Srivastava, S. S., and Prakash, S.: Simultaneous
 748 measurements of ammonia and nitric acid in ambient air at Agra (27°10'N and 78°05'E)
 749 (India), *Atmos. Environ.*, 35(34), 5979-5988, doi: 10.1016/S1352-2310(00)00394-0, 2001.

750 Perrino, C., Catrambone, M., Di Bucchianico, A. D. M., and Allegrini, I.: Gaseous ammonia
 751 in the urban area of Rome, Italy and its relationship with traffic emissions, *Atmos. Environ.*,
 752 36(34), 5385-5394, doi: 10.1016/S1352-2310(02)00469-7, 2002.

753 Phan, N. T., Kim, K. H., Shon, Z. H., Jeon, E. C., Jung, K., and Kim, N. J.: Analysis of
 754 ammonia variation in the urban atmosphere, *Atmos. Environ.*, 65, 177-185, doi:
 755 10.1016/j.atmosenv.2012.10.049, 2013.

756 Pierson, W. R., and Brachaczek, W. W.: Emissions of ammonia and amines from vehicles on
 757 the road, *Environ. Sci. Technol.*, 17(12), 757-760, doi: 10.1021/es00118a013, 1983.

758 Pierson, W. R., Gertler, A. W., Robinson, N. F., Sagebiel, J. C., Zielinska, B., Bishop, G. A.,
 759 Stedman, D., Zweidinger, R., and Ray, W. D.: Real-world automotive emissions-summary
 760 of studies in the Fort McHenry and Tuscarora Mountain tunnels, *Atmos. Environ.*, 30(12),
 761 2233-2256, doi: 10.1016/1352-2310(95)00276-6, 1996.

762 Pinder, R. W., Adams, P. J., and Pandis, S. N.: Ammonia emission controls as a cost-effective
 763 strategy for reducing atmospheric particulate matter in the eastern United States, *Environ.*
 764 *Sci. Technol.*, 41(2), 380-386, doi: 10.1021/es060379a, 2007.

765 Pio, C. A., Santos, I. M., Anacleto, T. D., Nunes, T. V., and Leal, R. M.: Particulate and
 766 gaseous air pollutant levels at the Portuguese west coast, *Atmos. Environ.*, 25(3), 669-680,
 767 doi: 10.1016/0960-1686(91)90065-F, 1991.

768 Polissar, A. V., Hopke, P. K., and Poirot, R. L.: Atmospheric aerosol over Vermont:
 769 Chemical composition and sources, *Environ. Sci. Technol.*, 35(23), 4604-4621, doi:
 770 10.1021/es0105865, 2001.

771 Pryor, S. C., Anlauf, K., Boudries, H., Hayden, K., Schiller, C. L., and Wiebe, A.: Spatial and
 772 temporal variability of high resolution reduced nitrogen concentrations in the Fraser Valley,
 773 *Atmos. Environ.*, 38(34), 5825-5836, doi: 10.1016/j.atmosenv.2003.12.045, 2004.

774 Reche, C., Viana, M., Pandolfi, M., Alastuey, A., Moreno, T., Amato, F., Ripoll, A., and
 775 Querol, X.: Urban NH₃ levels and sources in a Mediterranean environment, *Atmos.*
 776 *Environ.*, 57, 153-164, doi: 10.1016/j.atmosenv.2012.04.021, 2012.

777 Reche, C., Viana, M., Karanasiou, A., Cusack, M., Alastuey, A., Artiñano, B., Revuelta, M.,
 778 López-Mahía, P., Blanco-Heras, G., Rodríguez, S., Sánchez de la Campa, A., Fernández-
 779 Camacho, R., González-Castanedo, Y., Mantilla, E., Tang, S., and Querol, X.: Urban NH₃

780 levels and sources in six major Spanish cities, *Chemosphere*, 119, 769-777, doi:
781 10.1016/j.chemosphere.2014.07.097, 2015

782 Reis, S., Pinder, R., Zhang, M., Lijie, G., and Sutton, M.: Reactive nitrogen in atmospheric
783 emission inventories, *Atmos. Chem. Phys.*, 9(19), 7657-7677, doi: 10.5194/acp-9-7657-
784 2009, 2009.

785 Rodhe, L., Stintzing, A. R., and Steineck, S.: Ammonia emissions after application of human
786 urine to a clay soil for barley growth, *Nutr. Cycl. Agroecosys.*, 68(2), 191-198, doi:
787 10.1023/B:FRES.0000019046.10885.ee, 2004.

788 Salem, A. A., Soliman, A. A., and El-Haty, I. A.: Determination of nitrogen dioxide, sulfur
789 dioxide, ozone, and ammonia in ambient air using the passive sampling method associated
790 with ion chromatographic and potentiometric analyses, *Air Qual. Atmos. Health*, 2(3), 133-
791 145, doi: 10.1007/s11869-009-0040-4, 2009.

792 Sather, M. E., Mathew, J., Nguyen, N., Lay, J., Golod, G., Vet, R., Cotie, J. Hertel, T., Aaboe,
793 E., Callison, R., Adam, J., Keese, D., Freise, J., Hathcoat, A., Sakizzie, B., King, M., Lee,
794 C., Oliva, S., San Miguel, G., Crow, L., and Geasland, F.: Baseline ambient gaseous
795 ammonia concentrations in the Four Corners area and eastern Oklahoma, USA, *J. Environ.*
796 *Monit.*, 10(11), 1319-1325, doi: 10.1039/B807984F, 2008.

797 Saylor, R. D., Edgerton, E. S., Hartsell, B. E., Baumann, K., and Hansen, D. A.: Continuous
798 gaseous and total ammonia measurements from the southeastern aerosol research and
799 characterization (SEARCH) study, *Atmos. Environ.*, 44(38), 4994-5004, doi:
800 10.1016/j.atmosenv.2010.07.055, 2010.

801 Schlesinger, W. H., and Hartley, A. E.: A global budget for atmospheric NH₃, *Biogeochem.*,
802 15(3), 191-211, doi: 10.1007/BF00002936, 1992.

803 Seinfeld, J. H., and Pandis, S. N.: *Atmospheric chemistry and physics: From air pollution to*
804 *climate change*, Wiley, New York, 1998.

805 Sharma, S., Pathak, H., Datta, A., Saxena, M., Saud, T., and Mandal, T.: Study on mixing
806 ratio of atmospheric ammonia and other nitrogen components, *Proc. Int. Acad. Ecol.*
807 *Environ. Sci.*, 1(1), 26-35, 2011.

808 Shelef, M., and McCabe, R. W.: Twenty-five years after introduction of automotive catalysts:
809 what next?, *Catal. Today*, 62(1), 35-50, doi: 10.1016/S0920-5861(00)00407-7, 2000.

810 Shon, Z. H., Ghosh, S., Kim, K. H., Song, S. K., Jung, K., and Kim, N. J.: Analysis of water-
811 soluble ions and their precursor gases over diurnal cycle, *Atmos. Res.*, 132, 309-321, doi:
812 10.1016/j.atmosres.2013.06.003, 2013.

813 Singh, S., and Kulshrestha, U. C.: Abundance and distribution of gaseous ammonia and
 814 particulate ammonium at Delhi, India, *Biogeosci.*, 9(12), 5023-5029, doi: 10.5194/bg-9-
 815 5023-2012, 2012.

816 Singh, S., and Kulshrestha, U. C.: Rural versus urban gaseous inorganic reactive nitrogen in
 817 the Indo-Gangetic plains (IGP) of India, *Environ. Res. Lett.*, 9(12), 125004, doi:
 818 10.1088/1748-9326/9/12/125004, 2014.

819 Skamarock, W. C., Klemp, J. B., Dudhia, J., Gill, D. O., Barker, D. M., Duda, M. G., Huang,
 820 X., Wang, W., and Powers, J. G.: A description of the advanced research WRF version 3,
 821 NCAR Tech. Note, NCAR/TN-475+STR, 8 pp., Natl. Cent. for Atmos. Res., Boulder,
 822 Colo., 2008 (available at: http://www.mmm.ucar.edu/wrf/users/docs/arw_v3.pdf)

823 Stanier, C., Singh, A., Adamski, W., Baek, J., Caughey, M., Carmichael, G., Edgerton, E.,
 824 Kenski, D., Loerber, M., Oleson, J., Rohlf, T., Lee, S., Riemer, N., Shaw, S., Sousan, S.,
 825 and Spak, S. N.: Overview of the LADCO winter nitrate study: Hourly ammonia, nitric
 826 acid and PM_{2.5} composition at an urban and rural site pair during PM_{2.5} episodes in the US
 827 Great Lakes region, *Atmos. Chem. Phys.*, 12(22), 11037-11056, doi: 10.5194/acp-12-
 828 11037-2012, 2012.

829 Suarez-Bertoa, R., Zardini, A. and Astorga, C.: Ammonia exhaust emissions from spark
 830 ignition vehicles over the New European Driving Cycle, *Atmos. Environ.*, 97, 43-53, doi:
 831 10.1016/j.atmosenv.2014.07.050, 2014.

832 Suarez-Bertoa, R., Zardini, A. A., Lilova, V., Meyer, D., Nakatani, S., Hibel, F., Ewers, J.,
 833 Clairotte, M., Hill, L., and Astorga, C.: Intercomparison of real-time tailpipe ammonia
 834 measurements from vehicles tested over the new world-harmonized light-duty vehicle test
 835 cycle (WLTC), *Environ. Sci. Pollut. Res.*, 22(10), 7450-7460, doi: 10.1007/s11356-015-
 836 4267-3, 2015.

837 Sun, K., Tao, L., Miller, D. J., Khan, M. A., and Zondlo, M. A.: On-road ammonia emissions
 838 characterized by mobile, open-path measurements, *Environ. Sci. Technol.*, 48(7), 3943-
 839 3950, doi: 10.1021/es4047704, 2014.

840 Sutton, M., Dragosits, U., Y. Tang, and Fowler, D.: Ammonia emissions from non-
 841 agricultural sources in the UK, *Atmos. Environ.*, 34(6), 855-869, doi: 10.1016/S1352-
 842 2310(99)00362-3, 2000.

843 Sutton, M. A., Erisman, J. W., Dentener, F., and Möller, D.: Ammonia in the environment:
 844 from ancient times to the present, *Environ. Pollut.*, 156(3), 583-604, doi:
 845 10.1016/j.envpol.2008.03.013, 2008.

846 Tanner, P. A.: Vehicle-related ammonia emissions in Hong Kong, *Environ. Chem. Lett.*, 7(1),
 847 37-40, doi: 10.1007/s10311-007-0131-0, 2009.

848 Toro, R. A., Canales, M., Flocchini, R. G., and Morales, R. G.: Urban atmospheric ammonia
 849 in Santiago city, Chile, *Aerosol Air Qual. Res.*, 14(1), 33-44, doi:
 850 10.4209/aaqr.2012.07.0189, 2014.

851 Van Damme, M., Clarisse, L., Heald, C. L., Hurtmans, D., Ngadi, Y., Clerbaux, C., Dolman,
 852 A., Erisman, J., and Coheur, P. F.: Global distributions, time series and error
 853 characterization of atmospheric ammonia (NH₃) from IASI satellite observations, *Atmos.*
 854 *Chem. Phys.*, 14(6), 2905-2922, doi: 10.5194/acp-14-2905-2014, 2014.

855 Vogt, E., A. Held, and Klemm, O.: Sources and concentrations of gaseous and particulate
 856 reduced nitrogen in the city of Münster (Germany), *Atmos. Environ.*, 39(38), 7393-7402,
 857 doi: 10.1016/j.atmosenv.2005.09.012, 2005.

858 Walker, J. T., Whittall, D. R., Robarge, W., and Paerl, H. W.: Ambient ammonia and
 859 ammonium aerosol across a region of variable ammonia emission density, *Atmos. Environ.*,
 860 38(9), 1235-1246, doi: 10.1016/j.atmosenv.2003.11.027, 2004.

861 Wang, J., Xie, P., Qin, M., Ling, L., Ye, C., Liu, J., and Liu, W.: Study on the measurement
 862 of ambient ammonia in urban area based on open-path DOAS technique, *Spectrosc. Spect.*
 863 *Anal.*, 32(2), 476-480, doi: [http://dx.doi.org/10.3964/j.issn.1000-0593\(2012\)02-0476-05](http://dx.doi.org/10.3964/j.issn.1000-0593(2012)02-0476-05),
 864 2012.

865 Wang, S. X., Zhao, B., Cai, S. Y., Klimont, Z., Nielsen, C. P., Morikawa, T., Woo, J., Kim,
 866 Y., Fu, X., Xu, J., Hao, J., and He, K. B.: Emission trends and mitigation options for air
 867 pollutants in East Asia, *Atmos. Chem. Phys.*, 14(13), 6571-6603, doi: 10.5194/acp-14-
 868 6571-2014, 2014.

869 Wang, S. X., Xing, J., Jang, C. R., Zhu, Y., Fu, J. S., and Hao, J. M.: Impact assessment of
 870 ammonia emissions on inorganic aerosols in East China using response surface modeling
 871 technique, *Environ. Sci. Technol.*, 45(21), 9293-9300, doi: 10.1021/es2022347, 2011.

872 Wang, W., Wang, S., Xu, J., Zhou, R., Shi, C., and Zhou, B.: Gas-phase ammonia and PM
 873 ammonium in a busy traffic area of Nanjing, China, *Environ. Sci. Pollut. Res. Int.*, 9, 1-12,
 874 doi: 10.1007/s11356-015-5397-3, 2015.

875 Wang, Y., Zhang, Q. Q., He, K., Zhang, Q., and Chai, L.: Sulfate-nitrate-ammonium aerosols
 876 over China: response to 2000-2015 emission changes of sulfur dioxide, nitrogen oxides,
 877 and ammonia, *Atmos. Chem. Phys.*, 13(5), 2635-2652, doi: 10.5194/acp-13-2635-2013,
 878 2013.

879 Wei, S., Dai, Y., Liu, B., Zhu, A., Duan, Q., Wu, L., Ji, D., Ye, A., Yuan, H., Zhang, Q., Chen,
880 D., Chen, M., Chu, J., Dou, Y., Guo, J., Li, H., Li, J., Liang, L., Liang, X., Liu, H., Liu, S.,
881 Miao, C., and Zhang, Y.: A China data set of soil properties for land surface modeling, J.
882 Adv. Model. Earth Sy., 5(2), 212-224, doi: 10.1002/jame.20026, 2013.

883 Xiao, H. W., Xie, L. H., Long, A. M., Ye, F., Pan, Y. P., Li, D. N., Long, Z. H., Chen, L.,
884 Xiao, H. Y., and Liu, C. Q.: Use of isotopic compositions of nitrate in TSP to identify
885 sources and chemistry in South China Sea, Atmos. Environ., 109, 70-78, doi:
886 10.1016/j.atmosenv.2015.03.006, 2015.

887 Xiao, H. W., Xiao, H. Y., Long, A. M., and Wang, Y. L.: Who controls the monthly
888 variations of NH_4^+ nitrogen isotope composition in precipitation?, Atmos. Environ., 54,
889 201-206, doi: 10.1016/j.atmosenv.2012.02.035, 2012.

890 Xiao, H. Y., and Liu, C. Q.: Sources of nitrogen and sulfur in wet deposition at Guiyang,
891 southwest China, Atmos. Environ., 36(33), 5121-5130, doi: 10.1016/S1352-
892 2310(02)00649-0, 2002.

893 Yamamoto, N., Nishiura, H., Honjo, T., Ishikawa, Y., and Suzuki, K.: A long-term study of
894 atmospheric ammonia and particulate ammonium concentrations in Yokohama, Japan,
895 Atmos. Environ., 29(1), 97-103, doi: 10.1016/1352-2310(94)00226-B, 1995.

896 Yan, X., Akimoto, H., and Ohara, T.: Estimation of nitrous oxide, nitric oxide and ammonia
897 emissions from croplands in East, Southeast and South Asia, Global Change Biol., 9(7),
898 1080-1096, doi: 10.1046/j.1365-2486.2003.00649.x, 2003.

899 Yao, X., Hu, Q., Zhang, L., Evans, G. J., Godri, K. J., and Ng, A. C.: Is vehicular emission a
900 significant contributor to ammonia in the urban atmosphere?, Atmos. Environ., 80, 499-506,
901 doi: 10.1016/j.atmosenv.2013.08.028, 2013.

902 Ye, X., Ma, Z., Zhang, J., Du, H., Chen, J., Chen, H., Chen, H., Yang, X., Gao, W., and Geng,
903 F.: Important role of ammonia on haze formation in Shanghai, Environ. Res. Lett., 6(2),
904 024019, doi: 10.1088/1748-9326/6/2/024019, 2011.

905 Zhao, X., Xie, Y., Xiong, Z., Yan, X., Xing, G., and Zhu, Z.: Nitrogen fate and environmental
906 consequence in paddy soil under rice-wheat rotation in the Taihu lake region, China. Plant
907 Soil, 319(1), 225-234, doi: 10.1007/s11104-008-9865-0, 2009.

908 Zhao, Y., Zhang, J., and Nielsen, C.: The effects of recent control policies on trends in
909 emissions of anthropogenic atmospheric pollutants and CO_2 in China, Atmos. Chem. Phys.,
910 13(2), 487-508, doi: 10.5194/acp-13-487-2013, 2013.

911 Zhao, Y., Nielsen, C. P., McElroy, M. B., Zhang, L., and Zhang, J.: CO emissions in China:
 912 Uncertainties and implications of improved energy efficiency and emission control, *Atmos.*
 913 *Environ.*, 49, 103-113, doi: 10.1016/j.atmosenv.2011.12.015, 2012.
 914 Zheng, J., Ma, Y., Chen, M., Zhang, Q., Wang, L., Khalizov, A. F., Yao, L., Wang, Z., Wang,
 915 X., and Chen, L.: Measurement of atmospheric amines and ammonia using the high
 916 resolution time-of-flight chemical ionization mass spectrometry, *Atmos. Environ.*, 102,
 917 249-259, doi: 10.1016/j.atmosenv.2014.12.002, 2015.
 918 Zou, Z., Shan, F., Cai, Y., Chang, Y. H., and Zhao, Q.: Evolution of biomass burning on
 919 urban air quality: a case study of spring 2014 in Shanghai, *Environ. Monit. Forewarn.*, 4, 4-
 920 8, 2015. (in Chinese with English abstract)
 921

Table 1. Summary statistics of the NH₃ concentrations (µg m⁻³) measured in Shanghai during April 3, 2014-April 2, 2015. P10 and P90 represent the 10th and 90th concentration percentile, respectively.

	N	Mean	SD	Minimum	P10	Medium	P90	Maximum
All	8441	5.5	3.9	0.10	2.0	4.6	10.2	39.2
Spring	2198	5.1	3.8	0.10	1.7	4.1	9.6	25.1
Summer	2181	7.3	4.9	0.65	2.6	6.3	12.7	39.2
Autumn	1949	4.5	2.3	0.57	2.3	3.9	7.2	19.7
Winter	2113	5.0	3.4	0.43	1.8	4.3	9.3	30.7

940 **Table 2.** Ambient NH₃ concentration measurements in the urban atmosphere of China and
941 other countries/regions.

Location	Period	Methodology	Time resolution	Concentration (µg m ⁻³)	Reference
East Asia					
Shanghai, CN	2014.4-2015.4	MARGA online monitor	hourly	5.5±3.9	This study
Beijing, CN	2008.2-2010.7	Ogawa passive sampler	weekly	14.2±0.6 (2008), 18.1±13.8 (2009)	Meng et al., 2011
Beijing, CN	2007.1-2, 8	Annular diffusion denuder	daily	5.5±3.8 (winter), 25.4±6.9 (summer)	Ianniello et al., 2010
Xi'an, CN	2006.4-2007.4	Ogawa passive sampler	weekly	12.9/6.4/20.3 (annual/winter/summer)	Cao et al., 2009
Nanjing, CN	2012.8-9	HRTof-CIMS (a)	1 Hz	1.3±1.8 (industrial area)	Zheng et al., 2015
Nanjing, CN	2013.7-8	Portable NH ₃ online detector	hourly	6.7 (near road)	Wang et al., 2015
Guangzhou, CN	2010.11	OP-DOAS (b)	2.5 min	1.6	Wang et al., 2012
Urumqi, CN	2009.9-2010.8	Radiello passive sampler	biweekly	6.5	Li et al., 2013
Hong Kong, CN	2003.10-2006.5	Ogawa passive sampler	weekly	0.7 (rooftop) -7.1 (near road)	Tanner, 2009
Taichung, TW	2002.1-12	Annular diffusion denuder	12 h	8.5±3.0	Lin et al., 2006
Yokohama, JP	1987.1-1991.12	Glass flask sampling	3 h	2.5±1.4 (winter), 8.7±3.1 (summer)	Yamamoto et al., 1995
Nara, JP	1994.6-1995.5	Annular diffusion denuder	12 h	1.7 (winter), 1.6 (summer)	Matsumoto and Okita, 1998
Seoul, KP	1996.10-1997.9	Annular diffusion denuder	daily;	4.3/0.7/38.6 (annual/winter/summer)	Lee et al., 1999
Seoul, KP	2010.1-12	MARGA online monitor	hourly	6.8±3.3 (spring), 11.2±3.9 (summer)	Shon et al., 2013
Seoul, KP	2010.9-2011.8	MARGA online monitor	hourly	8.4±3.3	Phan et al., 2013
North America					
New York, US	1999.1-2000.6	Annular diffusion denuder	daily	5.0/4.1/6.1 (annual/winter/summer)	Bari et al., 2003
New York, US	2004.1-2	TDLAS (c)	<1 min	0.6 (winter)	Li et al., 2006
Chicago, US	1990.4-1991.3	Annular diffusion denuder	12 h	1.6±1.7	Lee et al., 1993
Pittsburgh, US	1993.7-9	Annular diffusion denuder	daily	3.9±4.4 (summer)	McCurdy et al., 1999
Los Angeles, US	1988.5-1994.9	Annular diffusion denuder	12 h	8.3	Blanchard et al., 2000
Sacramento, US	1988.10-1994.9	Annular diffusion denuder	12 h	9.5	Blanchard et al., 2000
Santa Barbara, US	1988.5-1994.9	Annular diffusion denuder	12 h	2.7	Blanchard et al., 2000
Farmington, US	2006.12-2007.12	Ogawa passive sampler	3 week	1.2±0.4	Sather et al., 2008
Clinton, US	2000.1-12	Annular diffusion denuder	12 h	2.6 (winter), 6.2 (summer)	Walker et al., 2004
Kinston, US	2000.1-12	Annular diffusion denuder	12 h	0.5 (winter), 2.7 (summer)	Walker et al., 2004
Morehead, US	2000.1-12	Annular diffusion denuder	12 h	0.3 (winter), 0.7 (summer)	Walker et al., 2004
Houston, US	2010.8	Quantum laser spectrometer	10 min	2.3±1.9 (summer)	Gong et al., 2011
Commerce, US	1978.11-12	Custumed passive sampler	two days	2.6 (winter)	Cadle et al., 1982
Vinton, US	1995.5-9	Ogawa passive sampler	biweekly	1.3±0.4 (summer)	Leaderer et al., 1999
Mexico city, MX	2006.3	Quantum laser spectrometer	6 min	17.7±1.0 (spring)	Fountoukis et al., 2009
Hamilton, CA	1992-1994	Annular diffusion denuder	daily	4.3	Brook et al., 1997
Europe					
Edinburgh, UK	2002.4-5	ALPHA passive sampler	bimonthly	4.8 (spring)	Cape et al., 2004
Münster, DE	2004.3-7	AMANDA (d)	10 min	3.9 (spring-summer)	Vogt et al., 2005
Toulouse, FR	1985.3-1986, 3	Nylon filter pack method	daily	3.8 (near road) – 19.8 (residential)	Giroux et al., 1997
Rome, IT	2001.5-2002.3	Annular diffusion denuder	30 min	17.2±2.7 (near road)	Perrino et al., 2002
Al-Ain, AE	2005.4-2006.4	Ogawa passive sampler	biweekly	9.7±4.8	Salem et al., 2009
Barcelona, ES	2011.5-9	AiRRmonia online analyzer	1 min	2.2±1.0 (near road), 5.6±2.1 (mixed)	Pandolfi et al., 2012
Barcelona, ES	2010.7, 2011.1	ALPHA passive sampler	biweekly	4.4 (winter), 9.5 (summer)	Reche et al., 2012
Barcelona, ES	2010.7, 2011.1	ALPHA passive sampler	biweekly	4.5±2.1 (winter), 9.2±6.6 (winter)	Reche et al., 2015
Madrid, ES	2011.3, 2011.7	ALPHA passive sampler	biweekly	2.3±1.3 (winter), 2.6±1.8 (summer)	Reche et al., 2015
Valencia, ES	2010.6, 2011.2-3	ALPHA passive sampler	biweekly	1.5±0.9 (winter), 0.5±0.4 (summer)	Reche et al., 2015
Huelva, ES	2010.11, 2011.5-6	ALPHA passive sampler	biweekly	2.8±3.8 (winter), 1.2±0.9 (summer)	Reche et al., 2015
Aveiro, PT	1988.8-1989.5	Nylon filter pack method	daily	3.5±1.9	Pio et al., 1991
South America					
Santiago, CL	2008.4-6	Ogawa passive sampler	monthly	15.0±3.8 (spring)	Toro et al., 2014
South Asia					
Lahore, PK	2005.12-2006.2	Annular diffusion denuder	12 h	50.1±6.9	Biswas et al., 2008
Dayalbagh, IN	1997.7, 1998.2	Annular diffusion denuder	3 h	12.5±2.2	Parmar et al., 2001
Delhi, IN	2008.9-10, 2009.9-10	Chemiluminescence analyzer	1 h	13.5±2.5 (2008), 14.4±3.7 (2009)	Sharma et al., 2011
Delhi, IN	2010.4-2011.11	Glass flask sampling	5 h	35.0±6.8	Singh and Kulshrestha, 2012
Delhi, IN	2012.10-2013.9	Glass flask sampling	8 h	40.7±6.8	Singh and Kulshrestha, 2014

Note: (a): High resolution time-of-flight chemical ionization mass spectrometry. (b): Open-path differential optical absorption spectroscopy. (c): Tunable diode laser absorption spectrometer. (d): Horizontal continuous-flow wet denuder.

Table 3. The average of temperature ($^{\circ}\text{C}$), relative humidity (%), accumulated rainfall (mm) and simulated planetary boundary layer (PBL) height (m) in Shanghai ($\text{mean} \pm 1\sigma$) during April 3, 2014-April 2, 2015.

	Temperature	Relative humidity	Accumulated rainfall	Simulated PBL height
All	17.1 ± 8.2	72.4 ± 16.1	1271.5	454.0 ± 309.2
Spring	16.1 ± 6.1	63.7 ± 19.5	298.3	448.8 ± 311.9
Summer	25.7 ± 3.4	78.4 ± 12.5	550.7	460.6 ± 293.2
Autumn	19.8 ± 4.4	76.5 ± 13.0	221.4	482.6 ± 321.6
Winter	6.7 ± 3.3	67.0 ± 15.6	192.1	428.0 ± 307.4

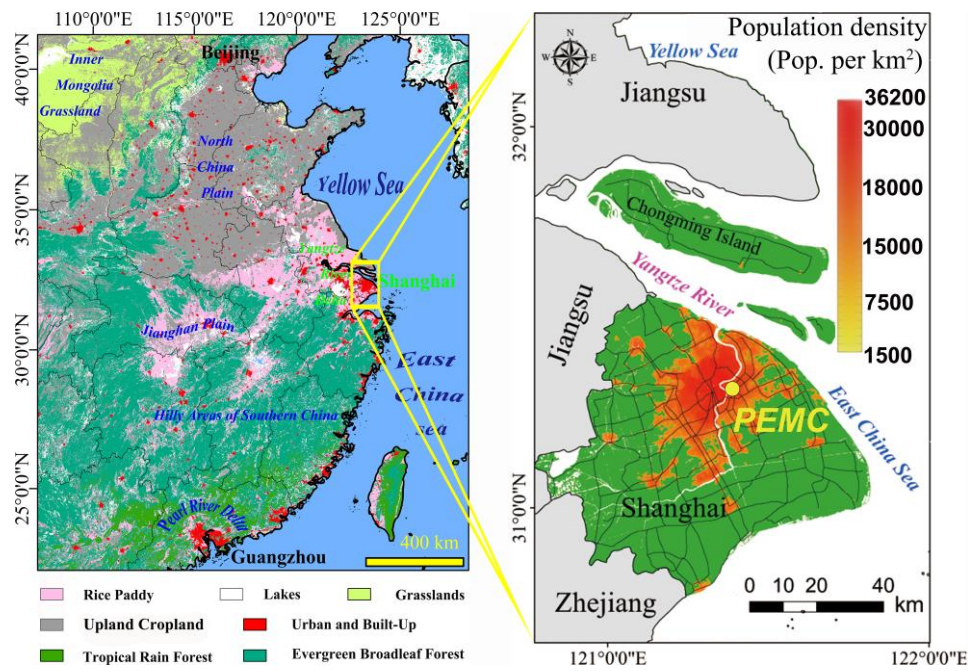


Figure 1. Location of the Pudong Environmental Monitoring Center (PEMC) supersite in Shanghai. The left panel shows various types of land use in eastern and southern China (adopted from (Broxton et al., 2014)). The red areas and black lines in the right panel represent the urban areas and main roads in Shanghai, respectively.

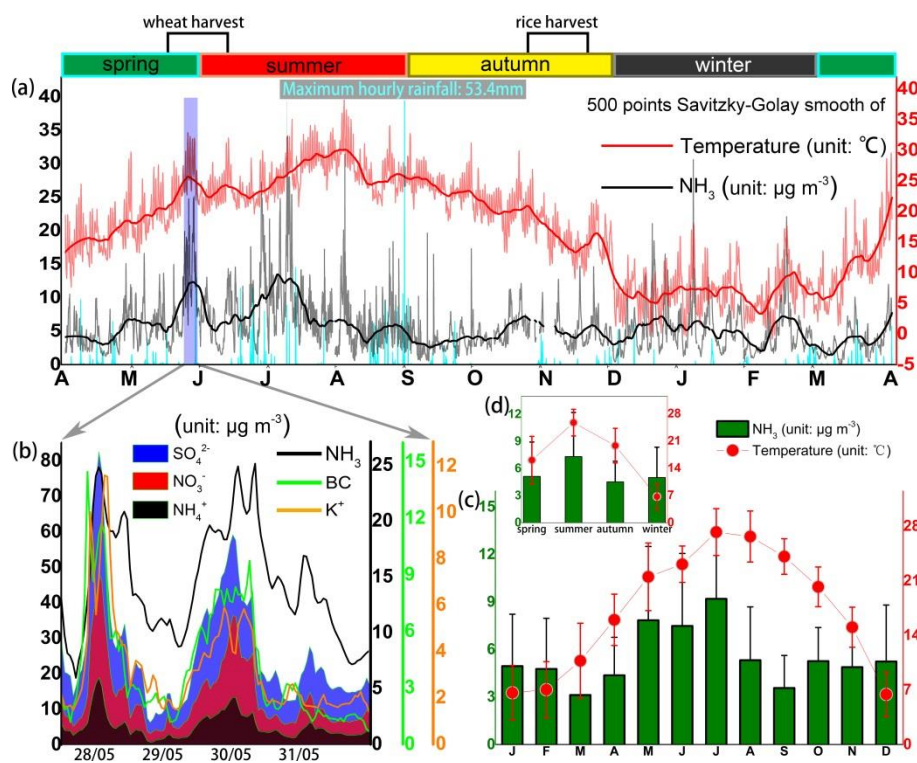


Figure 2. (a) Temporal variations of hourly NH₃ concentrations (gray) and temperature (red), along with 500-point Savitzky-Golay smoothed records in Shanghai from 3 April, 2014 to 2 April, 2015. Rainfall is shown in cyan. The vertical blue rectangle highlights NH₃ pollution episodes that occurred during the wheat harvest season. (b) Time series of NH₃, BC, SO₄²⁻, NO₃⁻, NH₄⁺, and K⁺ concentrations during periods of pollution associated with biomass burning. Monthly (c) and seasonal (d) variations of NH₃ average concentrations and temperature.

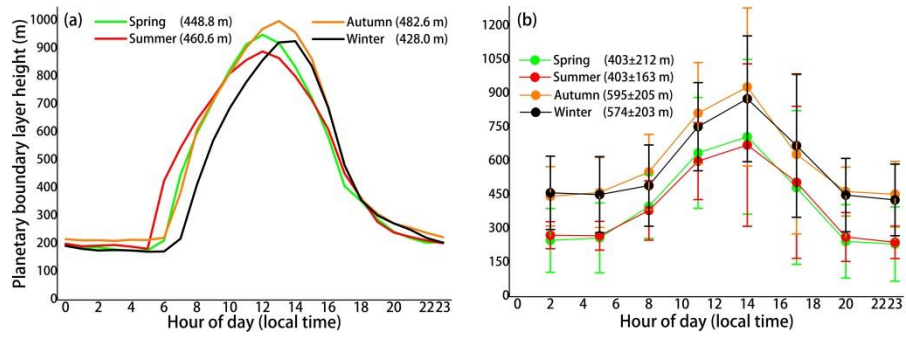


Figure 3. (a) Simulated diurnal profiles of the planetary boundary layer height in Shanghai during April 3, 2014-April 2, 2015. (b) Daily evolution of the planetary boundary layer height (NOAA READY achieved GDAS data) in Shanghai from 12 April, 2014 to 11 April, 2015. The number in the legend represents the average planetary boundary layer height, by time of day, in different seasons.

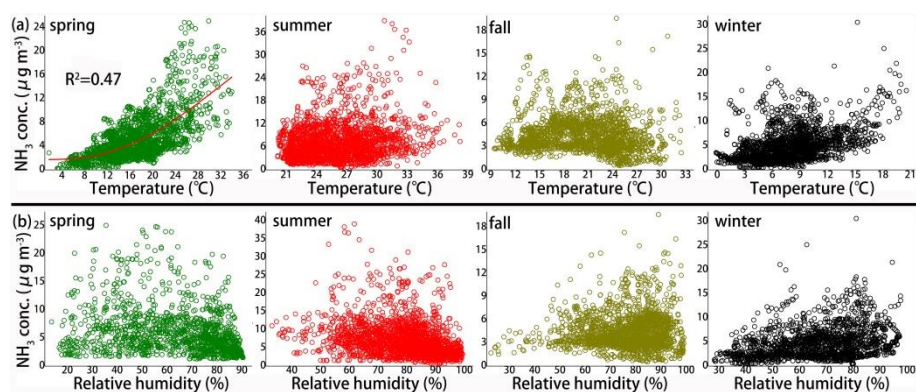


Figure 4. The relationship between hourly NH_3 concentration and hourly temperature (a) and hourly relative humidity (b) in four seasons at Pudong supersite between during April 3, 2014-April 2, 2015.

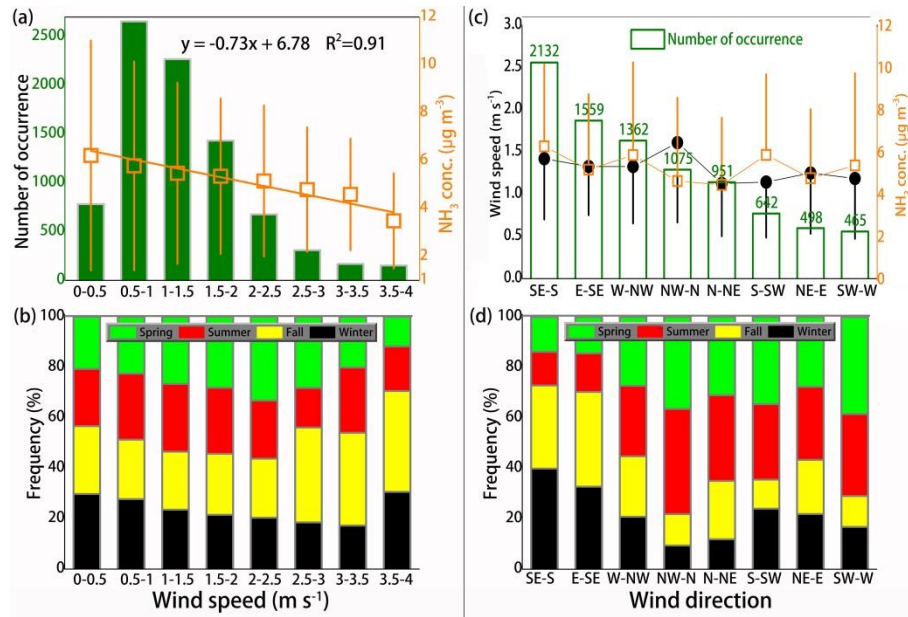


Figure 5. (a) Linear fitting of average NH₃ concentrations at different ranges of wind speed. The number of occurrences of wind (NOW) within each specific range of wind speed is shown as green columns. (b) Seasonal frequency distribution (%) of NOW at each specific range of wind speed. (c) The green boxes showing a descending order of the number of occurrences of wind at different wind directions. The points in black and the squares in orange represent the average wind speed and NH₃ concentration for each specific wind direction, respectively. (d) Seasonal frequency distribution (%) of NOW at each specific wind direction.

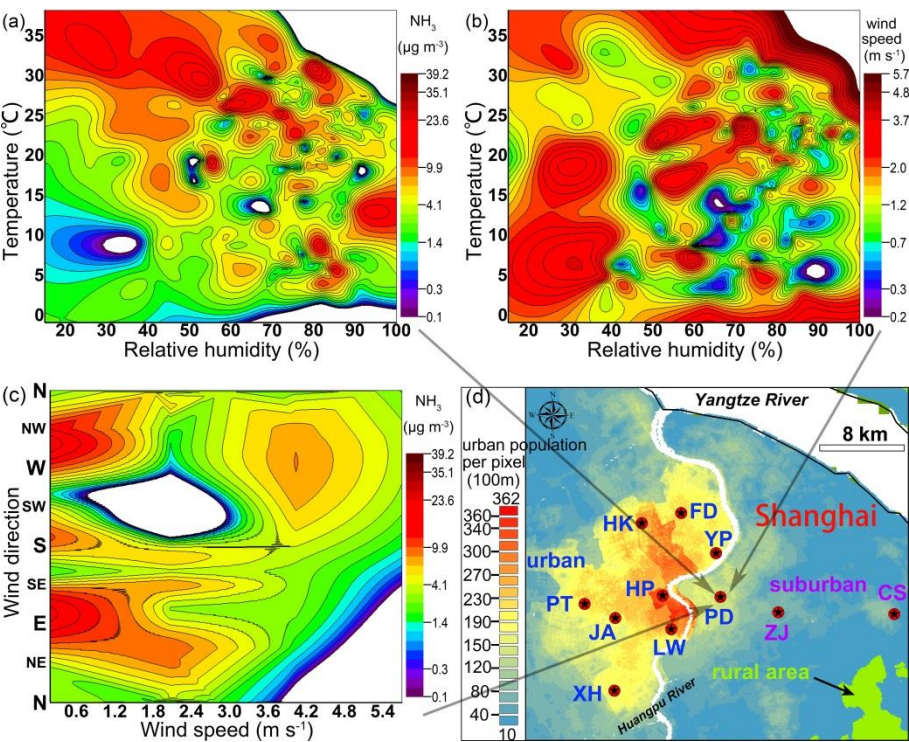


Figure 6. RH/T dependence of (a) NH₃ mass concentration and (b) WS, and (c) WS/WD dependence of NH₃ mass concentration at Pudong (PD) supersite for the year sampled. (d) The spatial distribution of environmental monitoring network in Shanghai. FD represents Fudan university. The base map is the 2010 urban population density, derived from a newly released high-resolution (100 m×100 m per pixel) population map of China (<http://www.worldpop.org.uk/>).

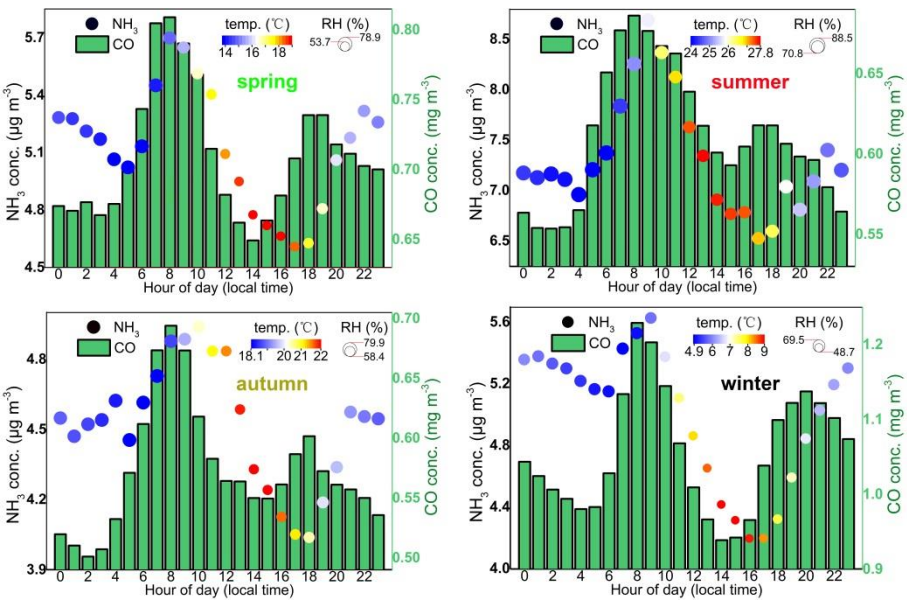


Figure 7. Seasonal diurnal profiles of NH₃ and CO concentrations in Shanghai. Color coded by hourly temperature and circle radius coded by hourly relative humidity.

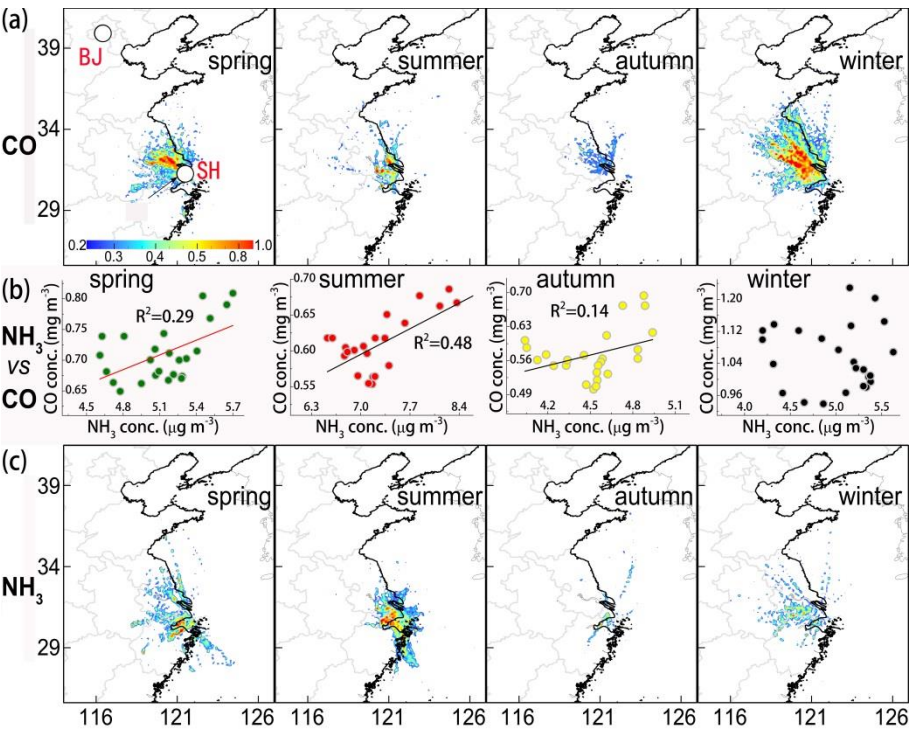


Figure 8. PSCF of CO (a) and NH₃ (c) during four seasons. The cities marked in each panel are Beijing (BJ) and Shanghai (SH). The color scales indicate the values of PSCF. (b) Relationship between hourly NH₃ and CO during four seasons.

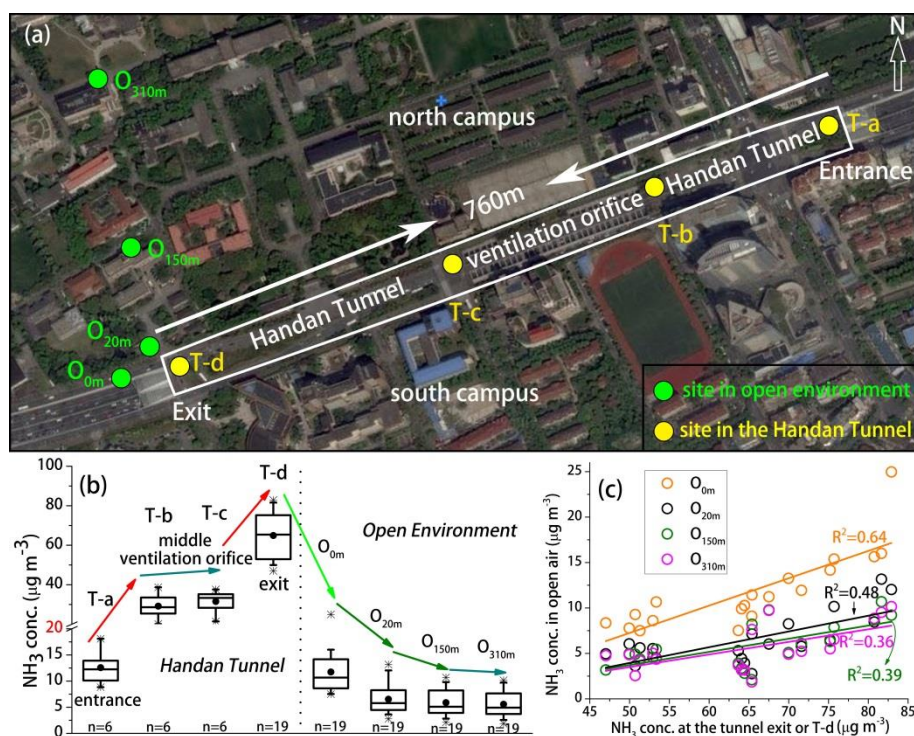


Figure 9. (a) Location of the eight sampling points (labeled in yellow; inside the tunnel from the entrance to the exit) and out (labeled in green; varying in distance from the tunnel) of the Handan tunnel where atmospheric concentrations of NH₃ were measured using fritted glass bubblers. The campus of Fudan University was separated into north and south parts by the tunnel. (b) Box-whisker plots of the NH₃ concentration sampled at each site, setting 20 as the breaking point of y axis. The box boundaries represent the 25th and 75th percentile, the horizontal line is the median, and the whiskers mark the 10th and 90th percentiles. (c) Relationship between the NH₃ concentration at T-d (the exit of the Handan tunnel) and the other four sites varying in distance from the Handan road in the open environment.